Analysis of the Application of Image-Forming Photosensors to Wide Field-of-View Daylight Star Trackers

TECHNICAL DOCUMENTARY REPORT NO. AL TDR 64-190

20 August 1964

AF Avionics Laboratory
Research and Technology Division
Air Force Systems Command
Wright-Patterson Air Force Base, Ohio

Project No. 4200, Task No. 420016

Prepared under Contract No. AF 33(657)-11694 by
Honeywell, Aeronautical Division, St. Petersburg, Florida)

DISCLAIMER NOTICE

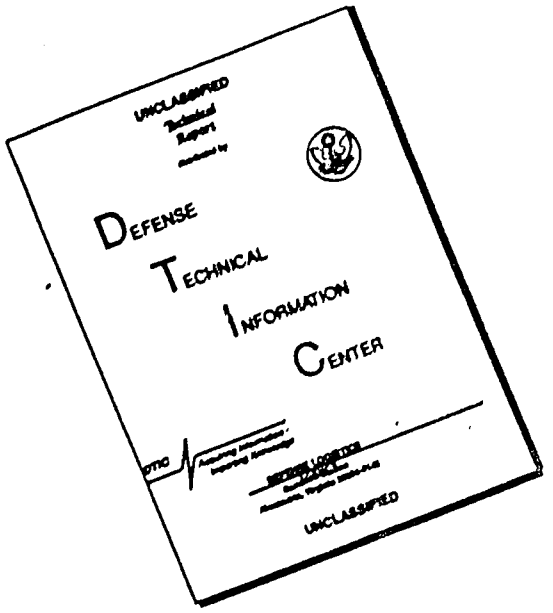

THIS DOCUMENT IS BEST QUALITY AVAILABLE. THE COPY FURNISHED TO DTIC CONTAINED A SIGNIFICANT NUMBER OF PAGES WHICH DO NOT REPRODUCE LEGIBLY.

NOTICES

When Government drawings, specifications, or other data are used for any purpose other than in connection with a definitely related Government procurement operation, the United States Government thereby incurs no responsibility nor any obligation whatsoever; and the fact that the Government may have formulated, furnished, or in any way supplied the said drawings, specifications, or other data, is not to be regarded by implication or otherwise as in any manner licensing the holder or any other person or corporation, or conveying any rights or permission to manufacture, use, or sell any patented invention that may in any way be related thereto.

Qualified requesters may obtain copies of this report from the Defense Documentation Center (DDC), (formerly ASTIA), Cameron Station, Bldg. 5, 5010 Duke Street, Alexandria, Virginia, 22314.

This report has been released to the Office of Technical Services, U.S. Department of Commerce, Washington 25, D. C., for sale to the general public.

Copies of this report should not be returned to the Research and Technology Division, Wright-Patterson Air Force Base, Ohio, unless return is required by security considerations, contractual obligations, or notice on a specific document.

FORWARD

This document reports the results of a study performed in fulfillment of Task 1, on contract AF 33 (657)-11694, " Advanced Celestial Tracking Instruments for Navigation".

This report was prepared by Bartley F. Conroy. The author acknowledges the assistance of Mr. R. W. Lowrie,* his supervisor, who contributed to the section on signal processing (Section 10.4), and to Mr. Willis Unruh* for orientation to this problem and critical review of the results.

AL TDR 64-189 "Design of a Pulse-Code Modulated Star Tracker", which was conducted concurrently under the same contract, has been published separately.

---

* Honeywell Aeronautical Division, St. Petersburg, Florida.

ABSTRACT

This report analyzes the performance limitations of wide field-of-view (approximately one degree by one degree) daylight startracking systems employing image-forming photosensors. The startracker was assumed to be an alignment reference for an inertial guidance system. Assumed system parameters are general enough to make results applicable to both air- and missile-borne applications, and to unrestricted operating altitudes.

TABLE OF CONTENTS

GLOSSARY OF SYMBOLS

A	Area - used in Section 6 for optical aperture area; also used in Section 8 for photodetector sensitive area.
$a \equiv$	$\frac{a}{a_{1/2}}$
a	Equivalent square image size.
$a_{1/2}$	Star optical image half-width.
B	Used interchangeably for image brightness and image illuminance.
ΔB	A relating change in brightness or illuminance.
b	A constant equal to $0.693 = \ln(0.5)$.
C, C_{th}	Threshold image contrast ratio. $C \equiv \frac{\Delta}{N_B}$
C_s	Star/sky image contrast.
$C_{m.s.}$	Measured star/sky contrast.
$C_{m.th.}$	Threshold measured contrast ratio.
C_e	Electronic noise contrast.
$C_{m.n.}$	Measured noise contrast for all noise except detector-scan noise.
c	Velocity of light in free space.
Δ	Object (star) luminance for a uniformly bright object.
D	Optical aperture diameter in inches.
D'	Optical aperture diameter in feet.
Δ_{eff}	Effective object luminance, defined by: $\Delta_{eff} \equiv C_{m.s.} N_B$.

GLOSSARY OF SYMBOLS (Continued)

ϵ_o	Luminous efficiency of a 2,870° K illumination source.
ϵ_B	Luminous efficiency of clear, daylight sky.
η	Optical system transmission coefficient.
f	Optical system focal length.
Δf	Bandwidth of the detector readout electronics.
g	Gain per stage of an electron multiplier.
$g(\alpha_1/2, x, y)$	Star optical image intensity distribution.
γ	Detector nonlinear response parameter, defined by: $I = RB^{\gamma}$
h	Planck's constant.
$h_\lambda (2870)$	Relative irradiance function of a 2,870° K blackbody.
$h_\lambda (T)$	Relative irradiance function of blackbody of temperature T.
$h_\lambda (B)$	Relative irradiance function of clear, daylight sky background.
H_{2870}	Peak irradiance of a blackbody of temperature 2,870.
H_0	Illuminance of a class AO, zero magnitude star.
H_T	Peak irradiance of a blackbody of temperature, T.
H_B	Peak irradiance of the clear daylight sky background.
Hs	True stellar illuminance.
Hs' =	η Hs
I_n	Image tube signal intensity after n^{th} readout.
G =	hc/λ'

GLOSSARY OF SYMBOLS (Continued)

I_n'		Image tube signal intensity before n^{th} readout. I_n and I_n' are related by: $\frac{I_n}{I_n'} = 1 - \frac{1}{p}$
i_n		Photodetector rms noise current.
i_{no}		Photodetector rms noise current for five megacycle bandwidth.
I		Output current from detector (general).
ΔI		A relative change in output current.
I_o		Signal current for an image tube in continuous operation at standard frame rate of 30/second.
I'		Output current from detector in unconventional operation viewing 2,370° K source.
K_m	$\equiv$	$(S/N)_{meas.}$
K_i		Minimum allowable measured signal-to-noise ratio.
L		Image illuminance.
ΔL		A relative change in illuminance.
$\ell(\lambda)$		Relative photopic sensitivity function.
ℓ_T		$\int_o^\infty h_\lambda(T) \cdot \ell(\lambda) \cdot d\lambda$
ℓ_B		$\int_o^\infty h_\lambda(B) \cdot \ell(\lambda) \cdot d\lambda$
ℓ_0		$\int_0^\infty h_\lambda(2370) \cdot \ell(\lambda) \cdot d\lambda$
L'		$\rho_{B0} \cdot L$
λ		Wavelength.
$\bar{\lambda}$		Average wavelength of detector response.
λ'		Average wavelength of photopic response ($\doteq$ 0.55 micron)

GLOSSARY OF SYMBOLS (Continued)

λ_1, λ_2 — Cutoff wavelengths for the photopic sensitivity curve.

λ_3, λ_4 — Cutoff wavelengths for the detector.

M^2 — Number of resolution elements of the detector. $M = \frac{\theta}{\alpha_{1/2}}$

M_s — Number of signal photons incident per unit time on detector.

M_B — Number of background photons per unit time incident on entire detector frame rate.

m_s — Stellar visible magnitude.

$m_{s.\,min}$ — Minimum stellar visible magnitude observable by startracker.

N_B — Sky luminance.

Ω — Field-of-view solid angle.

P_s — Power received from star.

$\frac{1}{p}$ — Fraction of image tube electronic image erased by readout, defined by:

$$(1 - \frac{1}{p}) = \frac{I_n}{I_{n-1}}$$

$q_0 \equiv \frac{I_0}{\tau_0}$; the magnitude of the electronic charge image on the retina of an image tube in continuous operation at 30 frames/second.

q_c — $\frac{Ic}{\tau}$; the magnitude of the electronic charge image on the retina of an image tube in continuous operation at a non-standard frame rate.

q' — $\frac{I'}{\tau'}$; the magnitude of the electronic charge image on the retina of an image tube in conventional operation ($\tau o \neq \tau \neq \tau'$).

η_d — Detective quantum efficiency-- defined as the square of the ratio of measured signal-to-noise ratio, $(S/N)_{meas.}$, to the ideal signal-to-noise ratio, $(S/N)_{ideal}$.

GLOSSARY OF SYMBOLS (Continued)

Q_R — Photocathode responsive quantum efficiency - defined as the number of countable photocathode output events per incident photon.

Q_R^0 — Photocathode quantum efficiency when continuously viewing a 2,870° K source at standard TV readout rate of 30 frames per second.

$$Q_R = (2870) = Q_R^0$$

Q_R^c — Photocathode quantum efficiency when continuously viewing a 2,870° K source at a non-standard readout rate.

$Q_R^0(B)$ — Photocathode quantum efficiency when viewing clear daylight sky background at 30 frames per second.

R — Detector responsivity defined by : $I = RB^{\gamma}$

R'' — Detector responsivity defined by : $I = R'' L^{\gamma}$

$$rT = \int_o^\infty r(\lambda) \cdot h_\lambda (T) \cdot d\lambda$$

$$rB = \int_o^\infty r(\lambda) \cdot h_\lambda (B) \cdot d\lambda$$

$$r_o = \int_o^\infty r(\lambda) \cdot h_\lambda (2870) \cdot d\lambda$$

$$\rho TB = \frac{r_T / r_B}{\ell T / \ell B} = \frac{1}{\rho BT}$$

$$\rho BO = \frac{r_B / r_0}{\ell B / \ell 0} = \frac{1}{\rho OB}$$

(S/N) — Signal-to-noise ratio.

$(S/N)_{ideal}$ — Signal-to-noise ratio in detection limited by background photon noise.

$(S/N)_{meas.}$ — Measured signal-to-noise ratio.

τ — Integration period of one resolution element.

GLOSSARY OF SYMBOLS (Continued)

τ_0	Standard television frame time (1/30 sec.)
τ'	Readout time for an image tube used in unconventional manner.
T	Stellar or blackbody radiation temperature.
θ	Field-of-coverage angular subtent, defined by: $\theta \equiv \sqrt{\Omega}$

INTRODUCTION

One approach to the solution of the daylight star tracking problem is to use optical-to-electronic image-transforming devices. The virtue of this approach lies partly in the flexibility such devices offer the system designer, and partly in the reduction of system noise. The successful application of this technique rests upon the system's ability to produce the necessary contrast between star image and bright sky background. It is the purpose of this document to describe the mission, and the mission environment, of a wide field-of-view (~ one degree by one degree) daylight star tracker, to identify the performance characteristics of an image-forming photosensor as dictated by the system's requirements, and assess, the adequacy of contemporary photosensors for this mission.

We hold ourselves to systems which operate in a non-tracking mode, that is, ones which indicate the coordinates of the star relative to the optical axis. These restrictions are fairly general and encompass quite a variety of applications, from preflight to in-flight calibration of inertial guidance systems in both ballistic missiles and aerodynamic cruise vehicles. The operating environment is restricted neither in altitude nor to any particular carrier vehicle.

SUMMARY

Primarily, two general classes of image-forming detectors are analyzed for their applicability to wide field-of-view daylight star trackers: those possessing memory (image storage capability), and; those without memory.

Equations describing the performance of single amplifier detectors without memory show that they are fundamentally limited by background photon noise. They were found to be incapable of low-altitutude (< 5, 000 feet) operation where detection of at least second magnitude stars against 1, 000 foot-lambert sky backgrounds is required, except for fields-of-view far less than one degree by one degree.

Multiple element detectors, with and without image storage capability, are presently under development which incorporate individual amplification for the elemental detector outputs. Ideally, these devices could detect dimmer than third magnitude stars against brighter than 2, 500 foot-lambert sky backgrounds. Practically speaking, however, their performance will be limited by noise in the switching circuitry required to multiplex the individual outputs into the signal processing subsystem. Assessment of performance of present devices of this type was not possible due to insufficient data available.

The memory-possessing, television image tubes on the other hand, in the ideal case of noiseless, flawless tubes offer the theoretical possiblity of detecting stars to roughly fifth magnitude against backgrounds of at least 2, 500 foot-lamberts. This was determined by calculations using derived system performance equations. These equations describe the performance of ideal image tubes in the detection of stellar images of low-to medium-contrast with the background (~1 percent to 75 percent contrast).

Practically speaking, however, internal noise, finite electron read-out beam size, and retina imperfections limit the performance of present-day television tubes less than the ideal. Methods of analyzing the limitations from such shortcomings were worked out. The performance of a system employing one of the most sensitive of contemporary vidicons was then calculated, revealing that detection of at least second magnitude stars in a one degree by one degree field-of-view against 1, 000 foot-lambert backgrounds was possible with an unsophisticated system. It is expected that more sophistication and ingenuity in system design, improved image tube production, increased knowledge of critical tube parameters, and statistical processing of the signal could significantly improve this to the point where fourth magnitude stars (or dimmer) may be detected against 2, 500 foot-lambert daylight sky backgrounds. Thus, performance at or near the theoretical limit possibly may be achieved.

Section 1

GENERAL STUDY CONSTRAINTS

The daylight star tracker is generally intended for use as a tactical, inertial navigation system alignment reference. It must be capable of operating in the worst tactical situation, bright daylight. It is assumed that the star tracker may utilize the inertial navigation system to stabilize its pointing direction. Since drift rates of such systems are much less than one arc-second per second of time, the star tracker's field of coverage is practically stationary during one frame time.

It is generally conceded that such a daylight star tracker must be able to detect stars of second to fourth magnitude and locate them in a field of view to an accuracy of a few arc-seconds (Reference 1). This would provide the inertial navigation system with at least two reference stars within a 105° cone anywhere on the celestial sphere (Reference 1).

It is preferable that the star tracker field-of-coverage be a cone with half angle greater than, or equal to, the uncertainty in alignment of the inertial-navigation system. If such is the case, the chosen star will be in the field-of-coverage the moment the system starts operating, eliminating the need for a search procedure. For an application such as initial, preflight or in-flight determination of the precise launching coordinates of a mobile ballistic missile, for example, this means a cone half angle of approximately one-half degree (Reference 1). Thus, we require for the star tracker system that it have a maximum field-of-view one degree by one degree.

To ensure that the study encompasses airborne applications, we adopt a reasonable upper limit on the optical aperture of four inches. Further, to ensure that the system be utilizable at any altitude we require operation against sky backgrounds of maximum luminance somewhere in the range 1,000 to 2,500 foot-lamberts (Reference 1, 2). In order that the system not be too slow, and require too high a degree of stabilization and too long a look-period, we adopt an upper limit of one second on the frame time. Also, since inertial navigation systems have bandwidths of about 30 cps or so, the star tracker frame time need not be less than about 1/30 second.

The short-frame-time, high-accuracy, and small-system size requirements limit the choice of electromagnetic spectral region for the star observations to the optical region (UV, Visible, and IR). Primary interest, therefore, centers in the spectral region from 0.4 to 1.0 micron, though there is some possibility that slightly longer or shorter wavelengths might become attractive in the future. However, present indications are that image-forming detectors for the infrared beyond one micron are not sensitive enough, while atmospheric interference plagues the very sensitive ultraviolet detectors operating at wavelengths below 0.4 micron.

The above considerations, outlining the scope of this study, are summarized as a set of system specifications in Table 1, below.

TABLE 1. GENERAL DAYLIGHT STARTRACKER SYSTEM SPECIFICATIONS

1.	Field-of-view:	
	a) maximum size	one degree by one degree
	b) motion (through stabilization of optical axis)	$\lesssim$ 3 arc-seconds
2.	Accuracy	$\lesssim$ 6 arc-seconds
3.	Optical system:	
	a) quality	diffraction limited
	b) aperture	2 to 4 inches
4.	Spectral region	Visible and near IR
5.	Sky background luminance (maximum)	1,000 to 2,500 foot-lamberts
6.	Minimum stellar magnitude	2nd to 4th magnitude

Section 2

STAR IMAGE PERTURBATIONS

Highest image/background contrast is theoretically achievable through the use of diffraction-limited optical systems. These are reasonably easy to obtain for apertures of two to four inches and for transmission somewhere in the spectral region from 0.4 to 1.0 micron. These will produce star diffraction images of three to six arc-seconds (angular subtent of the Airy disk).

In practice, under operational conditions, the diffraction-limited image may not be realized. Several phenomena conspire both to smear the image and cause it to dance about. The most notable of these, all of which have significant frequency components of one cps and higher, are listed below:

1. Servo stabilization loop transients induced by vehicle motion

2. Atmospheric shimmer

3. Aerodynamic turbulence

The first of these is a highly variable phenomenon dependent on the stabilization system characteristics and the state of motion of the vehicle. For the purposes of this paper it will be assumed to have a standard deviation of roughly ± six arc-seconds. This is the most serious image perturbation. Its effect will be ignored at the present, but methods of dealing with it will be discussed in subsection 9.8.

The last two effects have been investigated fairly extensively (References 3, 4, 5, 6, 7) and have been found to introduce image smearing both through image motion during the exposure period and through defocussing of the image caused by deformation of the star radiation wavefronts. These pheonmena typically have standard deviations of ± 1.5 arc-seconds or less. Thus, the half-width of the star diffraction image, and the standard deviations of the image-distorting phenomena (subparagraphs 1 and 2 above) are of approximately the same magnitude. In combination, their effects will be such as to increase the effective image size to an amount roughly double the diameter of the Airy disk of the star image. We may ignore these effects, then, in this initial analysis. However, bear in mind that the effects can reduce the resultant image contrast, since smearing of the star image over twice the diameter (or four times

the area) reduces the star image brightness by at most a factor of four, whereas the background image brightness is not affected. At any rate, the assumption of a diffraction-limited image is a good starting point, as the results may be readily extrapolated to realistic cases in a fairly straightforward manner. We will thus consider our analysis that of an "idealized system" in the sense that it views a stationary image and achieves resolution of that image to the diffraction limit. In subsection 9.7 we will discuss a method of achieving a very nearly diffraction-limited image, even in the presence of the above three perturbations.

Section 3

SKY BACKGROUND NOISE

Ideally, the daylight star tracker sees a star as a stationary, bright point of light against (in most cases) an even brighter background. The image on the photosensor of the weakest star of interest might be anywhere from six percent to 100 percent as bright as the brightest background. This background is not uniform but much experimental evidence (References 8, 9, 10) indicates its features do not contain any tiny discontinuities, having both the size of a star, and a brightness approaching fourth magnitude (relative to the rest of the background). Since the only images of interest are stars (we omit the planets), any bright spots of light much larger than a star image, such as a small, bright area in the sky, can be rejected by suitable electronic filtering of the signal output. We may thus conclude that false star targets due to bright spots in the sky background are not a problem.

Another type of noise, from the statistical fluctuation of the brightness of the background, will be important. In fact, it is inherent in any signal and cannot be eliminated. It thus determines the highest ratio of signal-to-noise any system can achieve. The rms value of the fluctuation in the number of photons arriving at the detector, during any given detection interval is equal to the square root of that arrival number.

The ideal signal-to-noise ratio achievable in detection of a given stellar body is determined by this noise and is given by:

$$\left(\frac{S}{N}\right)_{ideal} = \frac{M_S \tau}{\left(\frac{M_B}{M^2}\tau\right)^{1/2}} = \frac{M M_S \tau^{1/2}}{M_B^{1/2}} \qquad (3.1)$$

where

M_S = number of signal photons arriving per unit time.

M_B = number of background photons arriving per unit time.

τ = detection interval (image integration time of a resolution element).

M = photosensor resolution parameter. M^2 is the number of resolution elements on the photosensitive surface. Thus M_B/M^2 is the background photon arrival rate for a single resolution element.

Here it has been assumed that a resolution element is equal in size to the stellar image spot, and that the star energy is uniform over the spot. In Equation (3.1) note that if the system is limited by background statistical noise, the maximum signal-to-noise ratio depends directly on the number of resolution elements, M, of the photocathode. It is this dependence on M which makes it possible in some cases to decrease system noise. In other cases, however, this increase of $(S/N)_{ideal}$ is not realized for reasons which will become clear in Section 6.

Section 4

PHOTOSENSOR REQUIREMENTS

The heart of any star tracker is the photosensor which must detect with a high degree of probability the presence of the star image on its light-sensitive surface. For this study, it must also give the position of the image on its surface to an accuracy compatible with the star tracker's pointing accuracy which should be on the order of a few seconds of arc.

From the general considerations listed in Section 2 can be derived the approximate values of the important parameters of the photosensor. Table 4-2 gives an idea of the magnitudes of these parameters in an "idealized" detection situation. We assumed, for these calculations, a two-inch diffraction-limited optical system with a transmission spectrum from 0.4 to 0.8 micron and a 50 percent transmission loss, imaging a 1 degree x 1 degree field-of-view onto a 1 inch x 1 inch photocathode.

Note that the ratio of star image brightness to background brightness at the photosensor in the worst case is about 10 percent. This case represents detection of a fourth magnitude star against a 2,500 foot-lambert sky background, with a two-inch entrance aperture having a transmission loss of 50 percent. We shall continually refer to this particular combination of parameters in the remainder of the paper as the "worst case", since parameters represent the worst combination of system, background, and target parameters within the framework of this study. A more "typical mission", to which later reference is made, would be a 1,000 foot-lambert sky background, a second magnitude star, and a diffraction-limited, lossless, two-inch aperture optical system. The photocathode is assumed for the time being to have a spectral response matching the photopic sensitivity curve.

Detection of 10 percent image contrast is not exceedingly difficult though probably not an easy task if both high frame rates and a high confidence level are desired. It should be easy, however, to find a reasonable compromise between the extremes of the mission requirements and practical system performance. For example, if instead of a fourth magnitude star and a 2,500 foot-lambert background, we consider second magnitude and 1,000 foot-lamberts, star/background contrast increases to about 150 percent*. This will be considered "high" contrast. Of course, the

* Contrast is defined as the ratio of image luminance to background luminance. It should be noted that clear sky backgrounds over one-degree fields-of-view are fairly uniform. They typically display variations of less than a percent between regions a few arc-seconds apart. Thus, for example, a star image of a few arc-seconds angular size and 80 percent contrast represents a bright spot 80 times or more brighter than daylight sky variations of the same angular size.

TABLE 2. SOME PHOTOSENSOR DETECTION PARAMETERS FOR AN IDEALIZED SYSTEM

1.	Photosensor Time Constants	
	a. Image integration	$1/30 \text{ sec} \leq \tau \leq 1 \text{ sec}$
	b. Readout	$1/30 \text{ sec} \leq \tau' \leq 1 \text{ sec}$
2.	Photocathode illumination by background (1 in. x 1 in. photocathode):	
	a. 1,000 ft-lamberts sky luminance (1.58×10^{-3} watts/cm^2 ster)	0.15 ft-candles (0.24×10^{-6} watts/cm^2)
	b. 2,500 ft-lamberts sky luminance (3.94×10^{-3} watts/cm^2 ster)	0.38 ft-candles (0.60×10^{-6} watts/cm^2)
3.	Photocathode illumination by star image* (0.75×10^{-3} inches photocathode image):	

Effective Illumination**	Image Spot Illumination
a. 0.17×10^{-13} watts/cm^2 (4th magnitude) (1.1×10^{-8} ft-candles)	0.057×10^{-6} watts/cm^2 (0.036 ft-candles)
b. 1×10^{-13} watts/cm^2 (2nd magnitude) (6.8×10^{-8} ft-candles)	0.35×10^{-6} watts/cm^2 (0.22 ft-candles)
c. 6×10^{-13} watts/cm^2 (zero magnitude) (4.2×10^{-7} ft-candles)	2.2×10^{-6} watts/cm^2 (1.4 ft-candles)

4.	Image character	
	a. Size	Diffraction-limited(~2.72 arc-seconds half-width)
	b. Motion	Stationary
	c. Energy Distribution	Assumed uniform over diameter

*The value of 680 lumens/watt is the correct conversion factor for conversion of stellar irradiance to the photometric units for luminance.

**50% of the power has been subtracted for transmission losses.

previously mentioned image perturbations will tend to reduce this somewhat, so that we should consider the possibility of the star tracker having to deal with "medium" contrasts; that is, contrasts of 20 percent or so. Contrast of 5 percent or so will be considered "low". We conclude, therefore, that low to medium target-to-background contrast ratios should be assumed for the purposes of this study. Extreme cases in which contrast is very low can be alleviated somewhat within the range of variation of the mission requirements and system constraints. At the other extreme, cases of high contrast need not be analyzed as detection of such targets should be a relatively simple job, not requiring detailed analysis.

Section 5

THE AVAILABLE PHOTOSENSORS

Photosensors, currently available or in development which can give information on the position of point radiation images on their surfaces are of seven types:

1. Vidicon.
2. Image orthicon.
3. Image intensifier orthicon.
4. Image dissector.
5. Mosaics of single elements.
6. Electro-luminescent panels combined with single, large area, solid-state detectors.
7. Semiconductor point position indicators.

These devices can be separated into three classes, namely:

a. Image-forming photosensors without image storage capability*: this class contains types 4, 5, and 6.

b. Image-forming photosensors with image storage capability*: this class contains types 1, 2, and 3.

c. Others: type 7, for example.

Two recent developments in the camera tube field, the Ebicon, and the image Isocon will not be discussed in detail here. Their characteristics are very similar to the vidicon and image orthicon, respectively (References 11 and 12). Moreover, their sensitivities are roughly comparable to the image orthicon and image intensifier orthicon, respectively (References 11 and 12). Thus, these devices can be analyzed simply by slight extensions of the analyses of the vidicon and image orthicon.

---

*Ability to retain an image for an extended period after termination of exposure.

The first five types listed above will be considered more seriously here than the last two for the reasons outlined below. We must be aware first, though, that we may consider only multi-element photosensors with resolution capabilities approaching 600 to 1,200 lines -- that is, devices which could have from 360,000 to over 1,000,000 resolution elements.

The electro-luminescent panel (Item 7) is an image-forming photosensor still in the research and development stages. It is a large device, requiring a panel edge length of about 0.8 inch for each 100 resolution elements along an edge. A panel of a few hundred lines resolution, then, would measure several inches on an edge. Further, it has a longtime constant, requiring about one second to read out each 10^4 elements (100×100 elements square). Our requirements are for a minimum of 36×10^4 resolution elements to be read out in a maximum of one second. Thus, the present or near future electro-luminescent panels, besides being very large, are, at best, too slow. We will therefore not consider them further.

The last category represents a device which utilizes orthogonal currents in a semiconductor to determine the position of a spot of light on its surface (Reference 14). This device apparently would be confused by more than one target, and hence would have limited usefulness in a startracker. It has a low detectivity and resolution and initial calculations have indicated it cannot track second magnitude star targets with our assumed optical system limitations. We will therefore not consider it further.

Section 6

IMAGE-FORMING PHOTOSENSORS WITHOUT IMAGE STORAGE CAPABILITY

THE IMAGE DISSECTOR

The image dissector is basically a photomultiplier with provisions for imaging and deflecting the electrons emitted from the photosurface. The deflection system systematically scans the electron image of the light pattern on the photocathode past a mechanical aperture, and thus transforms a two-dimensional light pattern into a time-dependent electronic signal.

The image dissector has all the inherent capabilities of the photomultiplier. The photocathode response is fast, having a time constant well below one micro-second. Contemporary image dissector frame rates, however, do not utilize this fast response capability and usually do not exceed 1,000 per second. Resolution is good, approaching 1,000 lines per inch under certain conditions.

The image dissector, used in a daylight startracker, would be limited by statistical fluctuations in the brightness of the background*, and would be classed as a quasi-ideal detector (defined by R. Clark Jones (Reference 15) as one whose internal noise is insignificant in comparison to the statistical background noise). Many detectors are quasi-ideal in some detection situations but not in others. Some detectors never achieve this type of performance, as they have high internal noise levels and saturate before the background noise is high enough to compare to the detector noise.

It is instructive to examine the form of equation (3.1) for the quasi-ideal detector in general, and the image dissector in particular. Let us imagine that we have M resolution elements, a frame rate of m, and that the electronic information bandwidth of the photosensor readout is Δf. Then electrical bandwidth is related to M and m by:

$$\Delta f = \frac{1}{2\tau} = \frac{m M^2}{2} \qquad (6.1)$$

Combine this with Equation (3.1) to get:

$$\left(\frac{S}{N}\right)_{ideal} = \frac{M_s}{\sqrt{m M_b}} \qquad (6.2)$$

* or possibly by detector-scan noise of Subsection 7.9.

This equation will be of use to us in later discussions concerning the performance limitations of specific sensors. First, however, let us note in Equation (3), very curiously, that this ideal signal-to-noise ratio for detectors without memory is independent of the photosensor resolution parameter M. This can be understood by noting that statistical background noise increases as resolution goes down, due to the increased number of background photons collected by the larger resolution element. But the number of resolution elements in the (fixed) field-of-view, having decreased, a longer time interval, τ, is spent examining each resolution element, decreasing the information bandwidth needed. Thus, the ratio of the time per element, to the number of background photons per element, remains constant.

The significance of this independence of signal-to-noise ratio on resolution, for the quasi-ideal detector is rather interesting. For example, suppose that a photomultiplier is used in a detection situation in which the tube noise is well below the statistical background noise. Assume also that it is used only to indicate the presence of a star in a given field-of-view. Then an image dissector, having the same photocathode, could be employed for the same purpose, would achieve the same signal-to-noise ratio, and yield further information on the position of the star in the field-of-view.

The detective quantum efficiency, Q_D, is defined generally as the square of the ratio of the measured signal-to-noise to the ideal signal-to-noise in a given detection situation. For the image dissector Jones (Reference 15) shows that is essentially given by

$$Q_D = (1 - 1/g)\, Q_R \qquad (6.3)$$

Here Q_R is the photocathode responsive quantum efficiency, or countable events per incident photon. The quantity $1/g$ represents the noise contribution of the first dynode in the multiplier section of the tube.

Generally speaking, both the detective and the responsive quantum efficiency of a detector depend not only on the detector characteristics, but also on the manner in which it is used. In addition to detector characteristics, such things as overall spectral response of the detector and associated optical system, apparent spectral and spatial dependence of the irradiance of the object to be detected, frame rate, resolution, and electrical bandwidth are all important in determining the measured signal-to-noise ratio and, thus, quantum efficiency. Knowledge of all of these things is necessary before one can attempt to predict the detective quantum efficiency for a given detector in a given application.

From the definition of the detective quantum efficiency, and Equation (6.3), we find:

$$\left(\frac{S}{N}\right)_{meas} = \sqrt{\left|1 - \frac{1}{g}\right| Q_R} \left(\frac{S}{N}\right)_{ideal} \tag{6.4}$$

An expression for $(S/N)_{ideal}$, involving the pertinent system and radiation parameters, can be derived from Equation (6.2), and will be useful in comparing image dissector performance for given missions. This expression is:

$$\left(\frac{S}{N}\right)_{ideal} = H_s \sqrt{\frac{\eta A \bar{\lambda}}{m \Omega N_b h c}} \tag{6.5}$$

where:

η = optical system transmission coefficient

H_s = effective stellar irradiance

N_b = sky background radiance

A = optical aperture area

$\bar{\lambda}$ = average wavelength of detected light

m = frame rate

Ω = field-of-view solid angle for entire detector surface

h = Planck's constant

c = velocity of light

By substituting $(S/N)_{meas} = K_m$, and combining equations (6.4) and (6.5) we get:

$$K_m \doteq H_s \sqrt{\frac{\eta Q_R A \bar{\lambda} (1 - 1/g)}{m \Omega N_b h c}} \tag{6.6}$$

As a numerical example, consider the performance of the image dissector in the "typical mission", the parameters for which are listed below:

$H_s = 10^{-13}$ watts/cm^2 (average 2nd magnitude star)

N_b = 1,000 ft-lamberts = 5.2×10^{-4} watts/cm^2 ster

η = 1.0 (no optical transmission losses)

A = 25 cm^2 (about a 2-inch aperture)

Ω = 1 deg. x 1 deg. = 2.5×10^{-4} steradians

$\bar{\lambda}$ = 6,000 Å = 6×10^{-5} cm

Then by substitution of these into (7):

$$K_m \doteq 2.25 \sqrt{\frac{Q_R}{m}} \qquad (6.7)$$

Now, the responsive quantum efficiency, Q_R, by definition, can never exceed one. Also our minimum allowable frame rate, m, in this study is one. We therefore see that, in this typical case, the use of an idealized image dissector gives a signal-to-noise ratio of 2.25. This corresponds to a detection probability of 90 percent and false alarm fraction of 50 percent. The use of a four-inch aperture and a 0.9 deg. x 0.9 deg. field-of-view would increase the signal-to-noise ratio to four, giving a detection probability of about 95 percent and false alarm fraction of one percent (Reference 15).

The best value of Q_R for contemporary image dissectors is about 0.1, so that, in practice, in the typical case we could achieve a signal-to-noise ratio of four using a four-inch aperture and a 1/3 deg. x 1/3 deg. field-of-view.

We conclude this section by noting, then, that the performance of a daylight star tracker, as defined by the requirements in Table I, is marginal, even with the best available image dissectors, due to the rather low limit to the achievable signal-to-noise ratio, and to the small field-of-view limitations. Several research efforts are in progress to increase photoemissive device responsive quantum efficiencies. These can hope to increase the field-of-view, for the same S/N, to 0.9 deg. x 0.9 deg., or, by no more than about a factor of three if quantum efficiencies of 100 percent are realized. Therefore, mission performance, even with an ideal image dissector, would be marginal. It makes little sense to discuss other practical limitations of these devices, and the further deterioration in mission performance caused by them.

6.2 MOSAICS*

Mosaics of large numbers of elements are very difficult to fabricate, the main difficulty apparently being in making electrical contact by wire to each individual cell. The number of wires is so large as to pose formidable logistics, cross-coupling, and reliability problems. The fabrication of the cells themselves, by contrast, is quite simple. These are deposited as thin films on a suitable substrate. The present state-of-the-art in cell size is about 0.0015 inch, with a separation from its nearest neighbors of about 0.001 inch. Variation in sensitivity of ± 10 percent are typical from cell to cell. The largest mosaic fabricated to date has been 250 by 250, or 62,500 elements.

Aside from the problem of fabrication is the problem of readout of the mosaic. The use of an individual preamplifier for each cell with sequential sampling of the outputs is attractive as it allows the use of a narrow bandwidth for each individual detector. The microelectronic techniques for this type mosaic are presently under development in a number of laboratories. Generally, the output of the cells or individual preamplifiers is multiplexed sequentially, into one, or several preamplifiers. This technique appears to be developed to the point where readout of 10^6 elements in less than a second poses no problem. The cell wiring problem in large mosaics is so formidable that some manufacturers are going to electron beam readout techniques, thus eliminating the need for individual cells, and turning the mosaic into a continuous detector surface. Detectors are usually photovoltaic for this mode of readout and can incorporate a limited amount of image storage capability.

The performance of mosaics in wide field of view daylight star tracking will be analyzed by comparing the performance of 2 different types of mosaics: a mosaic having a single readout preamplifier which is multiplexed sequentially into each individual detector, and; a mosaic having an individual preamplifying arrangement for each detector element, but having a single final signal processing subsystem which is multiplexed sequentially into the amplified detector outputs.

One notices that mosaics having a single readout preamplifier in such a fashion that the bandwidth of the electronic readout circuitry is given by

---

*Most of the information on state-of-the-art mosaic developments was furnished by Dr. Gene Strull and Mr. Ed Erwin of the Westinghouse Air Arm Division.

Equation (6.1). We note further that such a mosaic has no image storage capability and would be a quasi-ideal detector if there were no cell noise present. Thus an upper limit to its performance can be obtained from the same equations as for the image dissector, with the omission of the dynode noise factor, 1/g. However, the quantum efficiency, Q_R, actually approaches very close to 1.0 for some semiconductor detectors at the peak wavelength of sensitivity. We thus conclude that the performance of an idealized mosaic with a single readout preamplifier in a daylight star tracker would be marginal just as with the image dissector. For most applications, field-of-view and other parameters would have to be further compromised to achieve the higher signal-to-noise ratios that the practical limitations of such a mosaic (e.g., cell noise and nonuniform response) would impose.

Mosaics having a separate amplifying circuit for each individual detector element may be designed with a time constant roughly equal to the frame time. The bandwidth of each circuit, in comparison with that of the single preamplifier used in the previous example for an entire mosaic, is quite small. This affords a reduction of detector, amplifier, and photon noise by 2 to 3 orders of magnitude. The signal, of course, for the same detection situation as for the previous example is increased by the gain of the individual amplifier. Thus the signal-to-noise ratio in the individual amplifier circuits can be very high, due to the amplified signal and reduced noise.

However, the individual outputs must now be fed sequentially into the single, signal processing subsystem amplifier. Thus the output impedance of each detector amplifier is the input impedance for the common amplifier in the signal processing subsystem. Since this amplifier necessarily has a wide bandwidth it is obvious that noise entering the signal at this point will be significant. In fact it will be of roughly the same magnitude as the preamplifier noise of the previous example.

We see then that the two types of mosaics described above in identical detection situations can be expected to yield different signal-to-noise ratios. The mosaics having individual amplification for each detector element can be expected to provide a signal-to-noise ratio, S/N, given roughly by:

$$S/N = \beta\,(S/N)_o \qquad (6.8)$$

where β = gain of the individual amplifiers.

$(S/N)_o$ = Signal-to-noise ratio for the mosaics having a single, common preamplifier.

A conservative value for the amplifier gain, β, is 50 or more; gains in excess of several hundred are not unreasonable. More gain can always be provided by additional stages of amplification.

We may substitute (6.6) for (S/N), and, using the same parameters as those in Section 6.1 arrive at:

$$S/N = 2.25\sqrt{\frac{Q_r}{m}} \qquad (6.9)$$

Allowing a quantum efficiency of 100%, and using a frame rate of 1 per second, equation (6.9) predicts a signal-to-noise ratio in excess of 40. This indicates that idealized mosaics employing individual amplification for each detector element could be capable of detecting, in a 1 degree field of view, second magnitude stars against a 1,000 foot lambert daylight sky. In fact they could possibly detect dimmer than 3rd magnitude stars against brighter than 2,500 foot-lambert skies.

The analysis above concerns mosaic performance limitations in a somewhat idealized case. It has not considered the practical limitations arising from noise introduced by multiplexing (switching), a necessary process with all mosaics. Switching at roughly megacycle rates is required. Unamplified signals from individual detectors is of the order a microvolt or so for silicon detectors, and higher for other types. Presently, switching noise at the required rates seems to be above one millivolt. This noise can be defeated if each detector output is individually amplified sufficiently to raise signal level above the switching noise. Thus the question of practical feasibility of such mosaics for daylight star tracking application rests upon two developments; low noise multiplexing for switching at megacycles rates, and; built-in individual amplification for the detector elements. The amplification required will depend on the degree to which switching noise can be suppressed. Sufficient data is not yet available on the characteristics developmental mosaics and switching techniques to allow an assessment of present performance.

Section 7

IMAGE-FORMING PHOTOSENSORS WITH IMAGE STORAGE CAPABILITY (CAMERA TUBES)

In beginning this section, note that the search for image-forming photosensors suitable to the performance of the daylight startracking missions encompassed by this study has been narrowed down to th information storing tubes, or television camera tubes (types 1, 2, and 3 of Section 5).

7.1 DAYLIGHT STARTRACKING AS AN UNCONVENTIONAL DAYLIGHT APPLICATION OF CAMERA TUBES

It is important to recognize that daylight startracking represents an unconventional mode of operation of camera tubes in the sense that it differs significantly from the conventional operating modes (broadcast television). The significant differences are:

1. Only small image detail (the "point" star image) is important, rather than both large and small detail.

2. The frame rate can be as low as one frame per second.

3. Low-, medium- and high-contrast objects (the star images) are viewed against a bright background. The brightness of this background cannot be controlled, as in the television broadcast studio.

The implication of these differences are that the interpretation and conversion of conventional image tube performance data for prediction of daylight startracker performance must be done with extreme care.

7.2 CAMERA TUBE TYPES

The information storage tubes to be considered are the vidicon, the image orthicon, and the image intensifier orthicon (which is an image orthicon preceded by one or more stages of image intensification). These devices are available for operation in any part of the spectral region from the near ultraviolet to the far infrared. To avoid confusion throughout our discussion of these devices, we will use the terminology "retina" to replace the more commonly used "target". A "target" in a camera tube is the surface upon which the electrical image of the field-of-view is produced.

Functional Similarity of Different Camera Tubes

Although the operation of the image orthicon is fundamentally different from that of the vidicon, both devices are functionally alike. Each has an image transducing section where a light image is transformed into an electrical image in the form of a voltage pattern. Also, each has a read-out section, consisting of a scanning electron beam. These electrons interact with the "retina", containing the stored electrical image, producing an electronic signal which may be amplified and then displayed. The image orthicon contains its own amplifier for this purpose (an electron multiplier), while the vidicon must utilize an external preamplifier. The image orthicon also incorporates part of a single-stage image intensifier in its image transducing section while the vidicon does not.

The image orthicon is analogous to a vidicon, with built-in image intensifier and very low-noise signal preamplifier. Therefore, we suspect that the image orthicon is a more sensitive device than the vidicon, while the image intensifier orthicon is still more sensitive. In practice this turns out to be true and is manifested both in the noise characteristics of the different types of tubes, and in the minimum illumination levels they are able to detect. For all this sensitivity, however, the image orthicon pays a penalty in physical size and in the added complexity of the necessary electrical circuitry to maintain its focussing, image intensifying, beam deflecting, and amplifying elements.

7.3 PHYSICAL SIZE OF CAMERA TUBES

The above analogy may be carried even as far as a quantitative comparison of physical size. The typical vidicon is 1-1/2 inches in diameter by 6-1/2 inches long and weighs about two ounces. A miniature version, half the above size, and requiring less operating electrical power, is available for compact, very light-weight TV cameras. An estimate of the image orthicon size is obtained by adding an image intensifier (3 inches diameter by 3 inches) in front of, and electron multiplier (2 inches diameter by 2-1/2 inches) behind the standard vidicon (1-1/2 inches diameter by 6 inches), arriving at nearly 12 inches length. Actually it is three inches in diameter over the front three inches of length, two inches diameter over the remainder, and the total length is closer to 13 inches. It weighs a minimum of 14 ounces (22 ounces for ruggedized versions). Performance of this type tube degrades, also, when a temperature gradient over 5°C exists between any two parts of the tube. Apparently no attempt has been made to miniaturize the image orthicon. Image intensifier orthicons are larger and heavier than image orthicons. The quality picture area on the vidicon is 1/2 inch by 1/2 inch square (1/4 inch on miniature version) while that of the image orthicon is 1.4 inches.

7.4 NOISE LEVELS

Vidicons, generally, have a higher level of internal noise than image orthicons. When viewing scenes at either low or high illumination, the lowest illumination detectable by vidicon imaging systems is set by noise in the preamplifier. Noise from the statistical fluctuations in the electron readout beam is below the level of the lowest-noise preamps. Thus, tube noise in vidicons is essentially dependent only on electrical bandwidth, not on magnitude of signal current. In image orthicons, however, electron beam noise is dominant, as noise from the electron multiplier is very low. The beam current (to within 10 percent) is practically independent of signal level. Thus internal noise in image orthicons is also essentially independent of signal level. In the image intensifier orthicon, the internal noise can be made lower than the statistical fluctuation in the number of signal photons detected by sufficient intensification of the image. Thus, the image intensifier orthicon may be classified as a quasi-ideal detector.

7.5 PHOTOCATHODE SENSITIVITIES

From Table 2 we see that daylight startrackers will be concerned with minimum photocathode illumination of about 0.01 foot candles. Vidicons, image orthicons, and image intensifier orthicons used conventionally for television broadcasting, together are capable of televising scenes with scene illumination ranging from direct sunlight ($\sim 10^4$ foot-candles) to completely overcast starlight ($\sim 10^{-5}$ foot-candles). The vidicon covers those scenes where photocathode illumination can be arranged to be 10^{-2} foot-candles or more. The image orthicon covers photocathode illumination levels to below 10^{-6} foot-candles, while the image intensifier orthicon extends the range to about 10^{-8} foot-candles. The range of operation of these devices overlap one another to some extent. Because of their extreme sensitivity, electrical complexity, and large size and weight, image intensifier orthicons are considered not applicable to daylight startracking problem under discussion.

7.6 IMAGE-STORAGE PROPERTIES (INTEGRATION)

Unconventional uses of vidicons and image orthicons ranges from military surveillance satellite systems and industrial process control, to scientific applications in astronomy and nuclear physics. Undoubtedly, the characteristic which makes them so versatile is their ability to store image information, that is, to integrate light intensity over variable periods. None of the devices is very good for frame times much less than 1/60 second due to a retention of the image known as "image lag". However, frame times of the order of tens of minutes can be realized. Again, the

image orthicon has the distinction of surpassing the vidicon in integrating ability. This ability is inherent in the very nature of the image transducing mechanisms of the two tubes.

The vidicon imaging section produces an electrical image by allowing a uniform layer of charge on the capacitive retina to leak through. The rate of leakage at any point is proportional to the radiation-induced change in resistance at that point. This change is, in turn, proportional to the light intensity at that point. The vidicon retina is necessarily, then, a leaky capacitor. Typical storage times of vidicons range from a few tenths of a second to a few minutes.

An image orthicon, however, produces an electrical image by producing electrical charge at any point on its retina at a rate proportional to the light intensity at that point. The light transducing property does not depend on a conductive mechanism so that a very high resistivity material is used, implying that the retina is a good (non-leaky) capacitor. Storage times for this device extend to nearly one hour.

Integration Mechanisms

Both the vidicon and image orthicon achieve image integration through two separate phenomena. The first type, "exposure integration", simply allows the electrical picture to build up in intensity during the exposure time. The second operates whenever camera tube readout incompletely erases the picture and may be understood by considering the following simplified example.

The image intensity gained in a single frame, say, is I (we assume that the scene is stationary over many frames). Thus, by the end of the first frame the retina leakage and the readout beam removes a fraction, $1/p$ of the picture leaving as remainder, I_1, given by:

$$I_1 = (1 - 1/p)I$$

During the next frame (assuming linearity) the image intensity builds up to I_2' which is:

$$I_2' = (2 - 1/p)I$$

After the second readout, the remaining intensity, I_2, is:

$$I_2 = (2 - 1/p)(1 - 1/p)I$$

This process continues until, during some frame, image intensity builds up to pI. The next readout then removes, ΔI_n, which is 1/p times the existing intensity, or:

$$\Delta I_n = \frac{1}{p} I_n' = \frac{1}{p} (pI) = I$$

This is exactly the amount to be gained during the succeeding frame, so that an equilibrium situation has been achieved. Accordingly, this type will be called "equilibrium integration". (Note that it takes many more than "p" frames to reach the equilibrium level.)

It appears, then, that utilization of exposure integration at a frame rate 1/p times the frame rate for equilibrium integration, with continuous readout, would achieve the same result in a shorter time. If leakage rates are low enough that image loss through this mechanism is not serious, this observation is approximately true (also, the slower scanning beam usually erases the image more completely than the fast-scanning beam and hence can be used at lower beam currents with an increase in resolution). The exposure method also has the advantage of reduced electrical bandwidth, and thus, lower noise.

Strictly speaking, both methods are operating simultaneously and rigorous analysis of the use of a given camera tube in a given situation should consider the effects of both leakage rate and image erasure as a function of scan rate. However for a system analysis, one can safely assume that either one method of integration, or the other may be used exclusively. "Exposure integration", with low leakage and complete erasure, is a reasonable assumption, since camera tube retinas for a system can be optimized for such performance at a given frame rate. Likewise, the camera tube retina could be optimized to operate in conjunction with a low current scanning beam which would purposely not fully discharge the image plate, yet not experience appreciable image loss due to leakage for the operational light levels to be encountered. This is, of course, equilibrium integration.

7.7 SPECTRAL RESPONSE

Spectral response characteristics of vidicons and image orthicons vary considerably. The image orthicon utilizes the same photoemissive materials as photomultipliers and is generally available with the same spectral response characteristics. Thus spectral sensitivity in image orthicons can be had anywhere in the spectral regions from the near ultraviolet (~ 0.1 micron) to the near infrared (~ 1.2 microns). Vidicons, on the other hand show very little variation in spectral response from one type of photocathode to another. They are essentially insensitive below

0.3 micron, peak at 0.4 to 0.6 micron and usually become insensitive past the red end of the visible spectrum at 0.7 micron. Efforts to extend sensitivity of the vidicon into the near infrared have resulted in photocathode materials having the same response at short-wave lengths. But, the peak response may occur between 0.6 and 0.7 micron, with the long-wave length sensitivity dropping off less rapidly. Residual sensitivity of about one percent at 2.0 microns has been achieved.

The spectral response of some vidicons also depends on the biasing potential of the retina. The whole spectral response curve apparently shifts toward the red (longer wave lengths) by about 500 Å when this potential is raised to a value permitting detection, by the tube, of the minimum illumination levels of which it is capable.

7.8 USABLE ILLUMINATION RANGES

A given vidicon can operate usefully for a fixed frame rate over a range of illumination of three orders of magnitude, though this is achieved only by adjustment of the bias potential on the retina. The useful range of illumination for the image orthicon is two orders of magnitude (also with bias adjustment). The operation of this type of tube is not completely understood. Alternative modes of operation as well as special techniques for dynamic range extension, low-contrast image enhancement, have been discovered (Reference 16, 17, 18), and may possibly prove to be useful in daylight startracking.

Very possibly, similar techniques for use with vidicons await discovery, though reference to any such work has not been found. Most of these techniques were discovered by astronomers through efforts to adapt the image orthicon to a variety of astronomical viewing conditions and celestial objects (Reference 16, 17, 18). They will not be discussed further here, but they should be given very serious study in any system where low-contrast targets are to be detected.

7.9 PHOTOCATHODE IMPERFECTIONS, IMAGE RESOLUTION, AND DETECTOR-SCAN NOISE

The resolution* of vidicons and image orthicons in conventional TV applications and in daylight startracking appears to be limited primarily by the size of the electron readout beam, and secondarily by the presence of image "graininess". Tube manufacturers have not produced readout beams

* Resolution in imaging systems depends both on the size of the object to be resolved, and contrast with its surroundings.

smaller than 5 by 10^{-4} inches. Image graininess results partly from grain structure in the photocathode, and introduces very fine grained variations (comparable in size to a star image) in the image of a uniformly illuminated scene. The brightness contrast of these variations is of the order of a few percent or less in both vidicons and image orthicons. Smoothly varying differences (shading) are also found when testing photocathode sensitivity along any given scan line on the surface. These can be held to less than 10 percent over the entire photocathode in quality tubes, and often are much less. These smoothly varying changes result in gross picture shading and, thus, low frequency video signals, which would be filtered out electronically in the startracker electronics (see Section 4 for allied discussion of this topic). Further image "graininess" results from the appearance of an image of the retinal mesh. This is a screen (with a maximum of 1,000 wires per inch in contemporary tubes) lying very close to the retina, which serves primarily to collect beam electrons which do not reach the retina, and secondary electrons ejected from the retina. The degree of contrast between the screen image and a uniform background image can be held to a few percent.

However, it has been shown that this contrast can rise to as much as 10 percent when the electron beam halfwidth is roughly equal to the mesh size. We conclude from this section that contemporary camera tube resolution could approach 2,000 lines per inch, and, for medium-, to high-contrast images is limited primarily by the electron beam size at the retina. Low-contrast image resolution would be limited by what we might call "detector-scan" noise or false signals arising from the scanning of the readout beam over photocathode imperfections and over the retinal mesh. The amplitude of this probably can be held to 10 percent or less.

A final characteristic which is a source of trouble in the use of camera tubes for any type of startracking is the occurrence of point-imperfections, or "hot-spots", on the photocathode. These are common to most vidicons. However, they can also occur in image orthicons. Such imperfections obviously occur also in the photocathodes of photomultipliers.

Point imperfections in vidicon photocathodes containing selenium compounds are quite notorious. They can result from a number of causes--most notably:

1. Surface contamination during manufacture.

2. Storage of tube at high temperatures, temperatures somewhat under 100° C are sufficient to induce point recrystallization.

3. Overexposure at points in an image during tube operation.

4. Too high image plate voltage during operation.

Some manufacturers claim the use of a different photocathode material alleviates this trouble. This other type of photocathode, they say, does not exhibit the tendency to recrystallize from the last three causes as does the selenium compound. Surface contamination hot spots can be controlled through special quality control during photocathode preparation.

Furthermore, the tubes can be selected to meet high quality specifications, with point imperfections held to amplitudes of about 10 percent or so of the background illumination. Further reduction of these irregularities is possible through the use of a tube faceplate mask. Such a mask would be made of a neutral density filter with transmissivity tailored to the tube irregularities.

The manufacturers claims do not seem to be firmly documented at this time and are based largely on the intuition and laboratory experience of their scientific development personnel. They have had little motivation to collect extensive data on such tube characteristics. However, in NASA's TIROS program a miniature RCA vidicon is utilized which meets specifications of no discernible hot spots larger than 0.0018 inch (Reference 22). However, the number of spots smaller than this runs on the order of a dozen. Minimum contrast defining a hot spot is estimated at 20 percent. RCA tube development personnel have indicated that, in their developmental photocathodes, hot spots less than 0.0018 inch in diameter show a maximum contrast below 10 percent. Information of this nature on the vidicons made by other manufacturers is not available at this time.

At any rate, the false star signals that would be produced by hot spots on the photocathode may not be a serious problem at all. Such false targets occur always at the same, known spots in the field-of-view. If they number only a dozen or less they can be eliminated by a very simple arithmetic calculation performed by the guidance system computer.

Section 8

DAYLIGHT STAR TRACKING PERFORMANCE OF A QUASI-IDEAL DETECTOR HAVING MEMORY (IMAGE STORAGE CAPABILITY)

We now enter into a discussion of the performance of a quasi-ideal detector which possesses a "memory", or image storage capability. An equation relating the ideal signal-to-noise ratio to the pertinent system, background, target, and photosensor parameters can be derived directly from Equation (3-1). The derivation is similar to that for Equation (6-5) with the exception that the detection interval is no longer the time the readout system spends interrogating one resolution element. The information storage capability of a detector possessing a memory makes the detection for each resolution element equal to the frame time, 1/m, assuming the integration process is linear in time. That this approximation is reasonable was established previously (see subsection 7.6).

8.1 THE CHARACTERISTIC EQUATION

The desired equation has also been derived by Rose (Reference 23) who has called it the characteristic equation, and is given by him in the form:*

$$N_B C^2 a^2 = \frac{G K_i^2}{\eta D^2 \tau Q_R} \qquad (8\text{-}1)$$

where:

N_B = scene luminance (considered uniform over the resolution element).

C = threshold contrast ratio = Δ / N_B.

a = angular subtent of a resolution element the element being square ($a^2 M^2$ = Ω in steradians).

$G = hc/\lambda' = 3.6 \times 10^{-19}$ joules

* We point out that Rose uses the word "brightness" for the photometric quantity "luminance". We will use the latter term since current workers in the field of photometry distinguish between the two, brightness being considered a visual attribute. Note also that we are using N_B, Δ, τ, and Q_R in place of Rose's B, ΔB, t, and θ, and have added the optical transmission coefficient, η, for completeness.

D = entrance aperture size

η = optical system transmission coefficient.

Δ = luminance of the object to be detected (the "target").

t = exposure time

K_i = minimum signal-to-noise ratio.* The subscript i denotes that the signal-to-noise ratio is that for the electronic current.

Q_R = quantum yield or, more correctly, photocathode responsive quantum efficiency.

8.2 SUPPLEMENTING THE CHARACTERISTIC EQUATION

Equation (8-1) must be supplemented in order to achieve our goals, as the minimum target irradiance is not explicit, its value being implied by the background radiance, contrast, and image size.

The Equation (8-1) predicts the threshold contrast for a target of fixed contrast, energy content of the image varying with target size. However, we wish to compare the performance of a quasi-ideal detector having memory, against a given target and background as the system and/or photosensor parameters are changed. We would like to supplement Equation (8-1) therefore, in such a way as to give information about the target star illuminance.

This is easily accomplished by noting that the ratio of star luminance to background luminance is the definition of stellar image contrast, C_s. That is:

$$C_s = \frac{\Delta}{N_B} \tag{8-2}$$

Also the power collected from the target star, P_S, is:**

$$P_S = N\frac{\Delta}{\pi}\,\frac{\pi D'^2}{4}\,a^2 \tag{8-3}$$

---

* Choice of actual signal-to-noise ratio determines detection probability, false alarm rate, and accuracy.

** We assume here, as did Rose in the derivation of Equation (8-1), that star image luminance is uniform over the square image.

Now, $4P_s/\pi D'^2$ is simply the effective stellar irradiance, H'_s. From Equations (8-3) and (8-2), we find the stellar irradiance corresponding to the contrast, C_S, as:

$$H'_S = \eta N_B C_S a^2 \tag{8-4}$$

Or, in terms of the true stellar illuminance, $H_S = H'_S/\eta$, the stellar image contrast is:

$$C_S = \frac{H_S}{N_B a^2} \tag{8-5}$$

Finally, we rewrite Equation (8-1) in the form:

$$C_{th}^2 = \frac{G K_i^2}{\eta N_B D^2 a^2 \tau Q_R} \tag{8-6}$$

Here we have appended the subscript (th) to C to emphasize that it represents the target background contrast which exists at detection threshold.

Equation (8-6) states that, once one choses the specific values for the system and photosensor parameters:

1. The minimum signal-to-noise ratio (K_i)
2. The optical aperture (D)
3. The uniform square-image size parameter, (a)
4. The photocathode responsive quantum efficiency, (Q_R)
5. The exposure time (τ), and,
6. The maximum background luminance against which the system must operate $(N_B)_i$

then, the threshold contrast, C_{th}, is completely determined. Equation (8-5) can then be used to calculate the minimum stellar irradiance necessary to produce this amount of contrast, and thus to determine the minimum stellar magnitude which can be detected with the degree of certainty required. Then Equation (8-5) may be written:

$$C_{th} = \frac{H_{s.\,min}}{a^2 N_B} \tag{8 5'}$$

Notice that Equations (8-5') and (8-6) can be combined in two different ways to eliminate* either C_{th} or $N_B a^2$. We will do this in subsection 8.3 for a specific calculation and to exhibit how N_B and H_S are related if all the system parameters are fixed. We prefer, however, to retain both equations in their present form for later use. Combining the two equations eliminates one or another of parameters which, although they may be unimportant in the quasi-ideal case, represent important parameters for the real detector. These parameters and their importance are discussed in Section 9.

8.3 "WORST" CASE CALCULATION FOR A LINEAR PHOTOSENSOR

As an example let us compute C_{th} from the following parameters, for the photosensor described in Table 2.

N_B = 2,500 foot-lamberts (the "worst" case background)

a = 1/20 arc-minute (this corresponds to approximately 1,200 line resolution)

η = 0.5

D = 2 inches

τ = 1/30 second

Q_R = 0.10 electrons/photon**

K_i = 6; (99 percent detection probability, false alarm rate 10^{-4})

We thus get:

$$C_{th}^2 = \frac{5 \times 36 \times 10^{-7} \times 400 \times 30 \times 10}{0.5 \times 25 \times 10^2 \times 4} = 4.32 \times 10^{-4}$$

Hence,

$$C_{th} = 2.08 \text{ percent} \qquad (8\text{-}7)$$

---

* N_B is eliminated only if Q_R is not a function of N_B. This happens to be true only for detectors with linear response.

** A rough evaluation of the product literature data on the RCA 2048A and the Machlett ML-7351 vidicon (Reference 24) tubes indicated a Q_R nearer 0.15 to 0.3. We have purposely used a more pessimistic value, in these calculations, of 0.1. This value is probably an upper limit for present image orthicons.

The worst case background presents, then, a threshold contrast for contemporary vidicons and image orthicons which is probably below the detector-scan noise produced by photocathode graininess and mesh image.

The minimum star irradiance which can be detected with the above-described background, contrast, detection probability and false alarm rate, can be computed from Equation (8-5) and is:

$$H_S = \frac{2.5 \times 10^3 \times 2.08 \times 10^{-2} \times 2.7 \times 10^{-8}}{4.00 \times 10^2}$$

or:

$$H_S = 0.35 \times 10^{-8} \text{ foot candles} \quad \text{(slightly brighter than magnitude)} \tag{8-8}$$

Notice now that Equations (8-5') and (8-6) may be equated to yield:

$$C_{th} = \frac{G K_i^2}{\eta D^2 H_S \tau Q_R} \tag{8-9}$$

which gives the threshold contrast once the system and photosensor parameters K_i, D, τ, and Q_R are given and the minimum star irradiance specified. Using the same parameters as in the previous example we use this equation to find the detection threshold contrast, with $H_s = 3.4 \times 10^{-14}$ watts/cm^2, that is, for a star of roughly fourth magnitude. Since starlight illumination represents 680 lumens/watt, we see that:

$$H_s = 2.2 \times 10^{-8} \text{ foot candles}$$

Thus:

$$C_{th} = \frac{1.35 \times 10^{-14} \times 36 \times 30 \times 10}{0.5 \times 4 \times 2.2 \times 10^{-8}} = 0.333 \text{ percent} \tag{8-10}$$

We see that the detection threshold contrast is even lower than in the previous case. The maximum allowable background luminance in this case is, from Equation (8-5):

$$N_B = \frac{3 \times 2.2 \times 10^{-8} \times 400}{10^{-2} \times 10^{-2} \times 2.7 \times 10^{-8}} = 100,000 \text{ foot-lamberts} \tag{8-11}$$

Finally, by combining Equation (8-6) and the square of Equation (8-5') we find that at threshold, the background luminance and the stellar target irradiance are related by:

$$N_B = \left(\frac{G \eta D^2 \tau Q_R}{a^2 K_i^2} \right) H_s^2 \text{min} \qquad (8\text{-}12)$$

This equation clearly indicates that if one views brighter stars (i.e. as star irradiance increases) the maximum tolerable background radiance increases.

Our calculation results; Equations (8-8), (8-10) and (8-11) clearly show that a quasi-ideal linear camera tube with t[illegible]ery reasonable system parameters chosen, diffraction-limited resolution, and stationary image, enables us to detect dimmer than fourth magnitude stars and to locate, by a quasi-ideal detector, to an accuracy of less than three arc-seconds, in a frame time of 1/30 second, against 2,500 foot-lambert daylight sky backgrounds, with a background-limited signal-to-noise ratio in excess of six. The assumed resolution was that of a diffraction-limited image. Image perturbation by the effects (2) and (3), mentioned in Section 2, cause the diffraction-limited resolution image of three arc-seconds to be smeared to six arc-seconds or so. Equations (8-5) and (8-6) then predict that in such a case, the stellar irradiance necessary to give detection with a minimum signal-to-noise ratio of six is 15 percent brighter than a fourth magnitude star. We may therefore feel confident that background statistical noise should present no problem in the detection of stars brighter than fourth magnitude against sky backgrounds not exceeding 2,500 foot-lamberts.* We have yet to calculate more accurate photosensor efficiencies, account for differences in spectral radiance between star, background, and detector calibration source, and determine the affect on detection of photosensor for nonlinear response, and use these to study other photosensor limitations on mission performance. This will be done in the following sections.

8.4 MODIFYING THE CHARACTERISTIC EQUATION FOR NONLINEAR DETECTOR RESPONSE AND SPECTRAL RADIANCE (EFFECTIVE TEMPERATURE) DIFFERENCES

8.4.1 Non-Linear Detector Response

We are interested now, in introducing into the characteristic Equation (8-6) the ability to handle photosensors with nonlinear response. This is

* These conclusions are based on a pessimistic value of Q_R and thus should be valid for the larger, more precise values.

readily accomplished by approximating the response with a power law; that is, one assumes the output current (not including the dark current), I, and the luminance of the objects occupying a resolution element in the field-of-view, B, are related by:

$$I = RB^{\gamma} \tag{8-13}$$

Also, since brightness and illuminance differ only by a constant factor:

$$I = R''L^{\gamma} \tag{8-13'}$$

where R, R'' and γ are parameters characteristics of the photosensor. In the case of the vidicon and the image orthicon, if R and γ are considered constant, Equations (8-13) and (8-13') are good to within about 5 percent.

Thus on a log I versus log B plot, the response is approximately a straight line of slope γ, or:

$$\log I = \log R + \gamma \log B = \log R'' + \gamma \log L \tag{8-14}$$

If we designate two points on the curve as (I, B) and (I + ΔI, B + ΔB), then we may also write:

$$\frac{\log (I + \Delta I) - \log I}{\log (B + \Delta B) - \log B} = \gamma \tag{8-15}$$

Thus:

$$\log \left(\frac{I + \Delta I}{I} \right) = \gamma \log \left(\frac{B + \Delta B}{B} \right)$$

or:

$$\log \left(1 + \frac{\Delta I}{I} \right) = \log \left(1 + \frac{\Delta B}{B} \right)^{\gamma}$$

$$\therefore \quad 1 + \frac{\Delta I}{I} = \left(1 + \frac{\Delta B}{B} \right)^{\gamma} \tag{8-16}$$

Using the binomial expansion for $(1 + x)^n$ we find that:

$$\frac{\Delta I}{I} = \gamma \left(\frac{\Delta B}{B} + \text{higher order terms in } \gamma \text{ and } \frac{\Delta B}{B} \right) \doteq \gamma \frac{\Delta B}{B} \tag{8-17}$$

If we neglect the higher order terms, we find that for $\gamma \simeq 0.75$ (typical of a vidicon) and for $\frac{\Delta B}{B} \lesssim 0.70$, the error in $\Delta I/I$ is less than 5 percent. As such, it is better than the assumption of constant γ in Equation (8-13). For the image orthicon, $\gamma \simeq 1.0$, for which case, Equation (8-17) is exact.

Hence, it is a very good analytical tool for the study of low-to-medium contrast relationships in camera tubes with nonlinear response representable as a power law. For high-contrast, the linear approximation gets bad but, for such contrast, there is little need for a performance analysis anyhow.

The incorporation of this result into the characteristic equation is simple now. We note merely that the contrast, C_m, actually measured by a camera tube is $\Delta I/I$. With Equation (8-17) this may be written:

$$C_m = \gamma \frac{\Delta B}{B} \tag{8-18}$$

What we have been calling the contrast is actually the "scene, or irradiance contrast". We now identify ΔB with our previous quantity Δ, and B with N_B. From Equations (8-18) and (8-2) it is obvious that the two are related by:

$$C_m = \gamma C \tag{8-18'}$$

The derivation of the characteristic Equation (8-6) should have required that the measured contrast, C_m, rather than the scene contrast, satisfy the threshold condition. (See Rose reference, Page 138.) We may thus modify the characteristic Equation (8-6) simply by replacing C (or C_{th}, as the case may be) by C_m.

That is:

$$C_{m.th}^2 = \frac{GK_i^2}{\gamma^2 \eta N_B D^2 a^2 \tau Q_R} \tag{8-19}$$

Equation (8-5), however, represents the scene contrast, C. Hence, from Equation (8-18'):

$$C_{m.s.} = \frac{\gamma H_s}{N_B a^2} \tag{8-20}$$

8.4.2 Modification for Different Effective Star and Background Temperatures

The contrast, C, between target and background, as defined by Equation (8-2), is valid only if it is assumed that the detector responds to a given amount of star illumination with the same output as it would respond to an identical amount of background illumination. This is not true if the star's effective spectral irradiance differs from that of the background. This situation can be corrected if the concept of contrast is replaced by that of "effective" or measured star contrast, $C_{m.s.}$, defined by:

$$C_{m.s.} = \frac{\Delta_{eff}}{N}$$

where:

N = effective background radiance (not luminance).

Δ_{eff} = effective star radiance (not luminance).

We would like to refer all radiation quantities to a common basis for comparison. For stellar-imaging applications involving detectors operating in, or very near, the visible region, illumination units are particularly suitable. If, then, Δ/N_B represents the visible illumination contrast, then the effective contrast will be:

$$C_{m.s.} \equiv \frac{\Delta_{eff}}{N} = \frac{\Delta}{N_B}\left[\frac{H_T \int r_\lambda h_\lambda(T) \cdot d\lambda}{H_B \int r_\lambda h_\lambda(B) \cdot d\lambda}\right]$$

The bracketed factor simply represents the effective star/sky contrast for the case when star and sky have equal luminance. Thus:

$$H_T \int \ell_\lambda \cdot h_\lambda(T) \cdot d\lambda = H_B \int \ell_\lambda \cdot h_\lambda(B) \cdot d\lambda$$

$$\therefore C_{m.s.} = \frac{\Delta}{N_B} \frac{r_T/r_B}{\ell_T/\ell_B}$$

The quantities r_T, r_B, ℓ_T and ℓ_B represent the integrals and are more fully defined in subsection 8.5 1, Equation (8-24). Comparing this equation with Equations (8-2), (8-5), and (8-20) we find that the measured star/background contrast $C_{m.s.}$ for a star of different radiation temperature than the background must satisfy:

$$C_{m.s.} = \frac{\gamma H_s}{N_B a^2} \times \left|\frac{r_T/r_B}{\ell_T/\ell_B}\right| \qquad (8\text{-}20')$$

The quantity, $H_s \frac{r_T/r_B}{\ell_T/\ell_B}$ represents the effective irradiance from the star producing photodetector response.

Equation (8-19) may be modified by noting that the measured threshold contrast should be written in terms of the effective sky background radiance, N, rather than the luminance, N_B. These are related by $N/N_B = r_B/\ell_B$. Thus Equation (8-19) may be written:

$$C_{m.th} = \frac{GK_i^2}{\gamma^2 \eta N_B D^2 a^2 \tau Q_R} \cdot \frac{\ell_B}{r_B} \qquad (8\text{-}19')$$

8.5 CALCULATION OF RESPONSIVE QUANTUM EFFICIENCY, Q_R, AND IMAGE SIZE, a

The two Equations (8-19') and (8-20') contain the pertinent system, photosensor, target, and background parameters that describe the performance of a daylight startracking system having a quasi-ideal image-forming photosensor possessing memory.

It is very instructive to choose specific values of γ, K_i, τ, and D, and then to construct on a plot of log C_m versus log $1/a$, the lines of constant N_B, as determined by Equation (8-19'), and the lines of constant H_s/N_B as determined by Equation (8-20').* We will defer this, however, until Section 9, where we will discuss a method of utilizing such a plot to describe the performance of real, memory-possessing, photosensors, after we have made certain modifications discussed below.

All of the parameters in Equations (8-19') and (8-20') are easily accessible with the exception of the responsive quantum efficiency, Q_R, and the resolution element size, a, (assumed equal to the image size). The following two paragraphs will discuss the calculation of these parameters.

8.5.1 Calculation of Responsive Quantum Efficiency When Viewing Sky Backgrounds

The responsive quantum efficiency, Q_R, is more elusive than the resolution parameter. It is generally not given by any manufacturer and thus must be deduced from other photosensor performance parameters. As pointed out previously in subsection 6.1, the value of the responsive

* This is an extension of the technique used by Rose (Reference 23).

quantum efficiency is characteristic of the situation in which it is used and depends on:

1. Overall spectral response of detector and associated optical system.

2. Apparent spectral irradiance of the target.

3. Spatial distribution of the apparent target irradiance.

4. Frame rate.

5. Photosensor spatial resolution.

6. Information processing bandwidth.

7. Other detector characteristics (e.g. electron beam accelerating potential, retina potential, etc.).

A sufficiently accurate value of the responsive quantum efficiency, Q_R, can be calculated if tube output current is known as a function of the source irradiance. Manufacturers supply a curve, known as the tube "transfer characteristic", which gives the output current as a function of photocathode illumination. To establish this curve, the camera tube photocathode (retina) is uniformly illuminated by radiation from a 2,870°K black body source. The tube output current is then measured directly with a microammeter at the output terminal of the retina, while the electron beam is scanning.

This curve may thus be considered as the signal output current for an image of a uniformly radiating 2,870°K square, gray body surface whose edge length is not less than three times the electron beam half-width. It is but a simple matter to convert the illumination scale to an irradiance scale, and further, to convert this scale to an appropriate one for irradiation by a source of a different effective radiating temperature. The factors calculated for converting the original transfer characteristic may then be applied to the calculation of responsive quantum efficiency for viewing a star against a bright sky background.

The responsive quantum efficiency, Q_R, appearing in the characteristic equation, is that for the detector when viewing the background. Thus, in this section, we will derive a formula for the responsive quantum efficiency of a camera tube when viewing a bright, daylight, sky background, in terms of the background illumination and effective radiation temperature, and the response characteristic of the photosensor chosen.

It is necessary to point out that the responsive quantum efficiency, Q_R, may be dependent on photocathode illumination if the tube response is non-linear ($\gamma \neq 1$). Thus we will derive a formula for Q_R which is valid for those tubes whose response satisfies the conditions necessary for the validity of Equations (8-13), (8-13') and (8-17). The derivation will be illustrated by calculations of Q_R for a vidicon. The derived equation must then be inserted into the characteristic Equation (8-19').

Consider the vidicon transfer characteristic* of Figure 8-1. At point P_1, the tube responsive quantum efficiency, $Q_R^O(2,870)$, may be calculated with sufficient accuracy from:

$$Q_R^O(2870) = \frac{I}{\eta LA} \quad \frac{\epsilon_0}{e} \quad \frac{hc}{\bar{\lambda}} \quad \frac{\int_{\lambda_1}^{\lambda_2} \ell_\lambda \cdot h_\lambda\,(2870) \cdot d\lambda}{\int_{\lambda_3}^{\lambda_4} r_\lambda \cdot h_\lambda\,(2870) \cdot d\lambda} \qquad (8\text{-}21)$$

where:

I = tube output current in amperes

L = photocathode illumination in foot candles

A = photocathode area in ft^2

ϵ_O = maximum luminous efficiency of the source under observation (lumens/watt)

e = electronic charge in coulombs

h = Planck's constant in joule-seconds

c = velocity of light in meters/second

$\bar{\lambda}$ = wavelength of average sensitivity of photocathode (in meters)

ℓ_λ = relative photopic sensitivity function

r_λ = relative photocathode spectral response function

* This transfer characteristic is that for the Machlett ML7351 vidicon (Reference 24). It is idealized in the sense of paragraph 8.4.2 where we found that, with little error, the transfer characteristic could be approximated by a straight line, of slope γ.

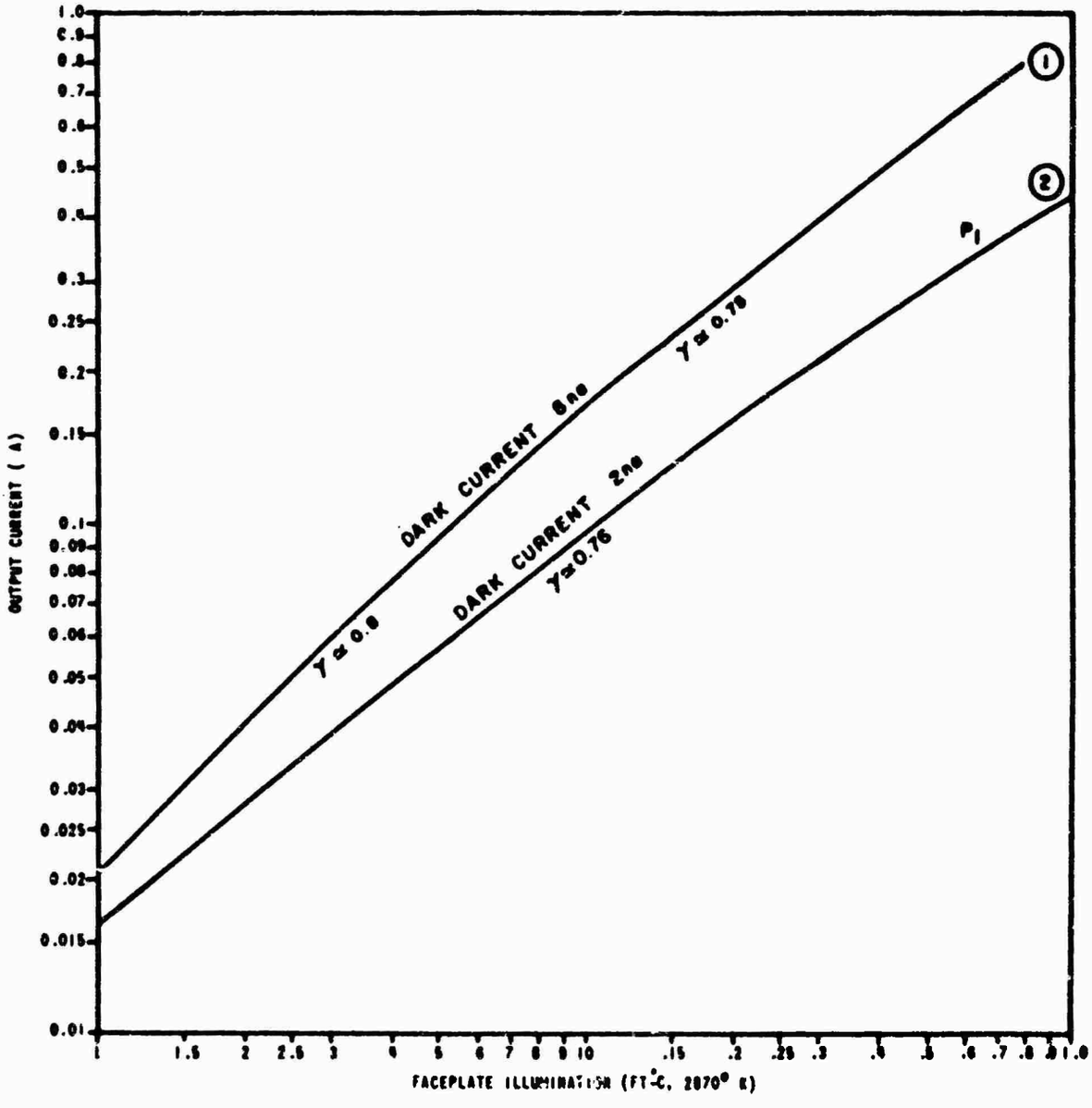
OUTPUT CURRENT (A)
FACEPLATE ILLUMINATION (FT-C, 2870° K)
DARK CURRENT 8nA
Y = 0.8
Y = 0.78
DARK CURRENT 2nA
Y=0.76
P1
1
2

h_λ (2870) = relative spectral irradiance function of a black body of temperature 2, 870°K

$\lambda_1, \lambda_2, \lambda_3, \lambda_4$ = cut-off wavelengths for visible region and for the photocathode

We will have need later of the functions $h_\lambda(T)$ and $h_\lambda(B)$ which will represent the relative spectral irradiance functions of a black body of temperature T, and of the bright sky background, respectively.

The parenthetical expression immediately following Q_R is simply to serve as a reminder that the quantity so calculated is dependent on the photocathode illumination as well as on the effective radiating temperature of the source.

The illumination is assumed (L) uniformly bright over the image. We emphasize the Equation (8-21) holds only for a source whose spectral radiance is that of a 2, 870°K gray body. $Q_R(T)$, for a gray body source of temperature, T, is given by the same equation except that $h_\lambda(T)$ replaces $h_\lambda(2, 870)$.

The last factor on the right side of Equation (8-21) takes account of the fact that the photocathode is sensitive to the source radiation in a different spectral region from that region which is used to calculate the source's effective visual illumination. Figure 8-2 illustrates this point. The area under the dashed curve C is proportional to the effective visual illumination from a 2, 870°K source while that under the solid curve D is proportional to the effective illumination producing a response at the photocathode.

Using the value of sky image brightness of 0.15 foot-candle, * taken from Table 2, and data from the transfer characteristic, Figure 8-1, we may evaluate Q_R (L 2, 870) for a contemporary vidicon. The values of the parameters in Equation 9-1 are:

η = 0.1

L = 0.60 foot-candle; $(0.94 \times 10^{-6}$ watts/cm$^2)$

I = 0.35×10^{-6} amperes (curve 2)

A = 2.78×10^{-3} ft^2; (5/8 inch by 5/8 inch)

* This brightness value must be increased due to the fact that the original calculation for Table 2 assumed the radiation was imaged onto a 1 inch by 1 inch photocathode, wheras the tube under consideration has only a 1/2 inch by 1/2 inch photocathode.

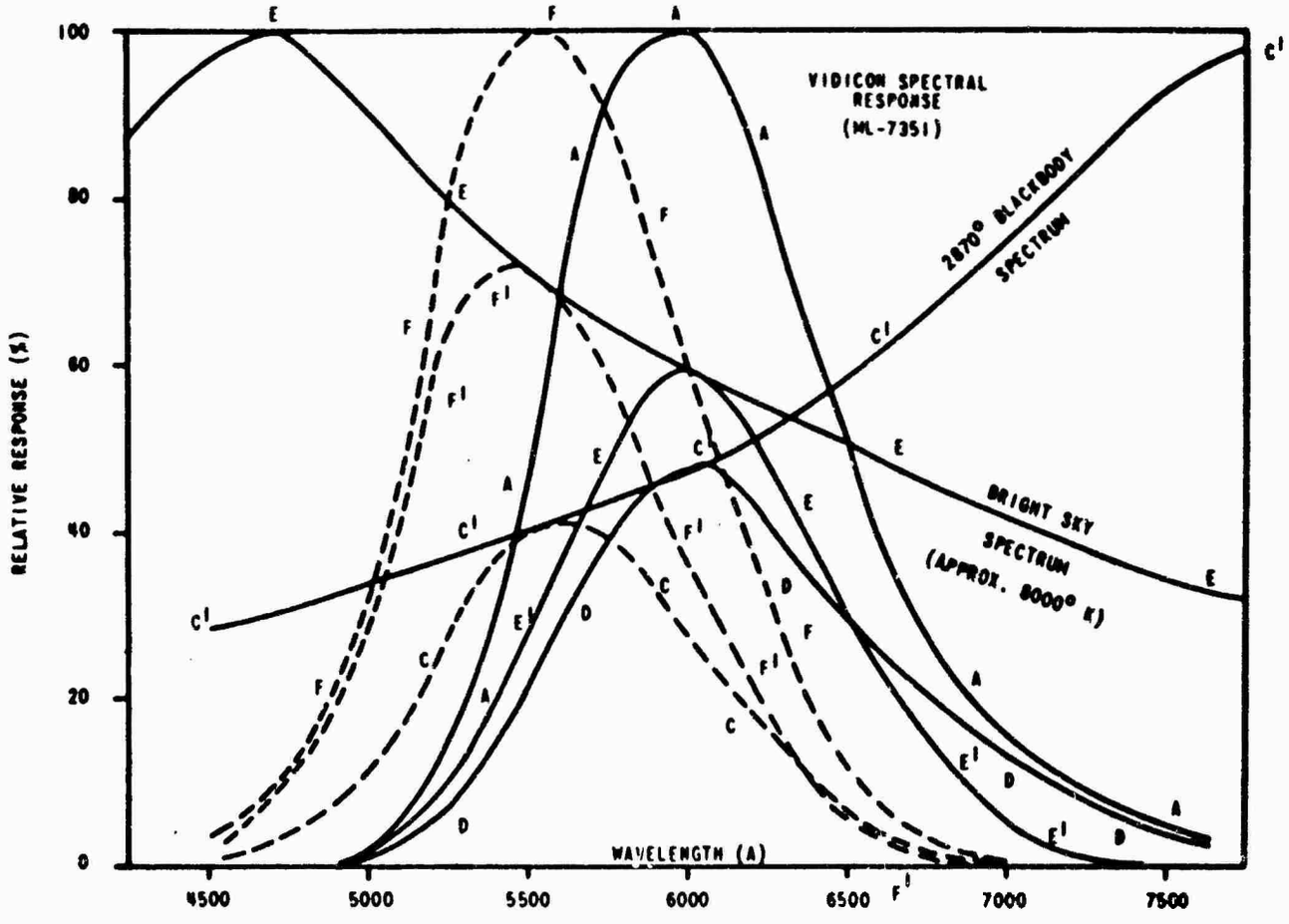

BRIGHT SKY SPECTRUM - CURVE E
2870° K SOURCE SPECTRUM - CURVE C'
SCOTOPIC SENSITIVITY - CURVE F (REF 25, P 6-140)
VIDICON SPECTRAL RESPONSE - CURVE A (REF 24)
VIDICON RESPONSE TO BRIGHT SKY - AREA UNDER CURVE E'
ILLUMINATION FROM BRIGHT SKY - AREA UNDER CURVE F'
VIDICON RESPONSE TO 2870° K - AREA UNDER CURVE D
ILLUMINATION FROM 2870° K - AREA UNDER CURVE C

$$\frac{\int_{\lambda_1}^{\lambda_2} \ell_\lambda \cdot h_\lambda (2,870) \cdot d\lambda}{\int_{\lambda_1}^{\lambda_2} r_\lambda \cdot h_\lambda (2,870) \cdot d\lambda} \doteq 0.75$$

ϵ_C = 510 lumens/watt; (Reference 25)

Thus:

$$Q_R(2870) = \frac{0.25 \times 10^{-6} \times 510 \times 6.6 \times 10^{-34} \times 3 \times 10^{8}}{0.385 \times 2.78 \times 10^{-3} \times 1.6 \times 10^{-19} \times 6 \times 10^{-7}} \times \frac{\text{electrons}}{\text{photon}}$$

$$= 0.165$$

It is necessary to recognize that the quantum efficiency of an image tube, when used in an unconventional manner, is not necessarily the same (for the same illumination level) as it is when used in a conventional manner. In conventional usage, the tube is exposed continually to the scene being viewed, while in unconventional usage it may be exposed for a short period, and then obscured during the readout. This important operational difference must be taken into account. It should be noted that the quantum efficiency of a linear detector is independent of radiant intensity. Only detectors with non-linear response show a dependence of quantum efficiency on radiant intensity.

The photocathode responsive quantum efficiency of an image tube in conventional operation viewing a uniformly bright background, illuminated by a 2,870°K source, is easily determined as a function of photocathode illumination from the tube transfer characteristics (see Figure 8-1). Q_R^0 will be directly dependent on the ratio of output current to photocathode illumination. We may write:*

$$Q_R^0 \sim \frac{q_0}{\int_0^{\tau_0} L \cdot d\tau} \sim \frac{q_0}{L\tau_0} \sim \frac{I_0 \tau_0}{L\tau_0} = \frac{I_0}{L} \qquad (8\text{-}21a)$$

where I_0 is signal current, τ_0 is readout exposure time, and q_0 is total retina charge. Now, if while operating with continuous exposure, one changes the exposure time to a value τ, from the conventional value, τ_0 (τ_0 = 1/30 second), then the total detected radiant energy is changed in the ratio τ/τ_0. Thus, for continuous operation, the quantum efficiency, Q_R^c at non-standard frame rates is given by:

$$Q_R^c \sim \frac{q_t}{\int_0^{\tau} L \cdot dt}$$

* Note that L is a constant, independent of time, t.

q_c being the total accumulated charge. For nonlinear detectors, one can easily demonstrate that:

$$\frac{q_0}{q_c} = \left(\frac{\tau_0}{\tau}\right)^{\gamma} \tag{8-21b}$$

where I_0 and I_c are the signal current amplitudes.

$$\therefore\ Q_R^c \sim \left(\frac{\tau}{\tau_0}\right)^{\gamma} \frac{q_0}{L\tau} = \frac{q_0}{L\tau_0} \left(\frac{\tau_0}{\tau}\right)^{1-\gamma} = \left(\frac{\tau}{\tau_0}\right)^{1-\gamma} Q_R^0 ; \tag{8-21c}$$

That is, the quantum efficiency of an image tube being continuously exposed is changed by a change in frame rate.

Consider, now the tube which is exposed for a period, τ, and interrogated during a period τ'. Then the quantum efficiency, Q_R, will be:

$$Q_R \sim \frac{q'}{\int_0^{\tau} L \cdot dt} = \frac{q'}{L\tau} \tag{8-21d}$$

q' being the total accumulated charge in this case. It should be obvious that q' is equal to q_c. That is:

$$\frac{q'}{q_c} = 1 \tag{8-21e}$$

From Equations (8-21b, c, and d) then:

$$Q_R = \left(\frac{\tau_0}{\tau}\right)^{1-\gamma} Q_R^0 \tag{8-21'}$$

In other words, operation of the tube, with readout time differing from exposure time, does not change the quantum efficiency from the case of continuous operation (with the same exposure time).

However, the output currents do not behave in the same fashion. We note that:

$$\frac{I_0}{I_c} = \frac{q_0/\tau_0}{q_c/\tau_c} = \frac{\tau}{\tau_0} \frac{q_0}{q_c}$$

which, from Equation (8-21b) becomes:

$$\frac{I_0}{I_c} = \left(\frac{\tau}{\tau_0}\right)^{1-\gamma} \tag{8-21f}$$

Also note that:

$$\frac{I'}{I_c} = \frac{q'/\tau'}{q_c/\tau}$$

Substituting from Equation (8-21e):

$$\frac{I'}{I_c} = \frac{\tau}{\tau'} \qquad (8\text{-}21g)$$

Thus, from Equations (8-21f and g):

$$I' = \frac{\tau}{\tau'}\left(\frac{\tau_0}{\tau}\right)^{1-\gamma} I_0 = \frac{\tau_0}{\tau'}\left(\frac{\tau}{\tau_0}\right)^{\gamma} I_0 \qquad (8\text{-}21h)$$

We must now determine what happens to Q_R^0, if we substitute a gray body background of a different temperature, T_B, but having the same effective visual illumination as the 2,870°K calibration source. We note first that for a background having the same visible luminance as a 2,870°K black body:

$$H_{2,870} \int_{\lambda_1}^{\lambda_2} \ell_\lambda \cdot h_\lambda (2,870) \cdot d\lambda = H_B \int_{\lambda_1}^{\lambda_2} \ell_\lambda \cdot h_\lambda (B) \cdot d\lambda \qquad (8\text{-}22)$$

Thus:

$$H_{2,870}/H_B = \int_{\lambda_1}^{\lambda_2} \ell_\lambda \cdot h_\lambda (B) \cdot d\lambda \Big/ \int_{\lambda_1}^{\lambda_2} \ell_\lambda \cdot h_\lambda (2,870) \cdot d\lambda \qquad (8\text{-}23)$$

$$= \ell_B/\ell_0$$

Here we have made the substitutions:

$$\left.\begin{aligned} \ell_B &= \int_{\lambda_1}^{\lambda_2} \ell_\lambda \cdot h_\lambda (B) \cdot d\lambda \\ \ell_0 &= \int_{\lambda_1}^{\lambda_2} \ell_\lambda \cdot h_\lambda (2,870) \cdot d\lambda \end{aligned}\right\} \qquad (8\text{-}24)$$

In the ensuing discussion we shall, for brevity, use the symbols ℓ_T, r_B, r_0, r_T, all of which are defined by equations similar to Equation (8-24).

Since effective visual illumination of the calibration source and the sky backgrounds is to be the same, then the ratio, ρ_{B0}, of the effective radiant energy producing tube response for the sky background source of temperature B, to that from the calibration source of temperature 2,870°K is:

$$\rho_{B0} = \frac{H_B \int_{\lambda_1}^{\lambda_2} r_\lambda \cdot h_\lambda (B) \cdot d\lambda}{H_{2,870} \int_{\lambda_1}^{\lambda_2} r_\lambda \cdot h_\lambda (2,870) \cdot d\lambda}$$

Substituting from Equation (9-6):

$$\rho_{B0} = \frac{\int_{\lambda 3}^{\lambda 4} r_\lambda \cdot h_\lambda (B) \cdot d\lambda}{\int_{\lambda 3}^{\lambda 4} r_\lambda \cdot h_\lambda (2,870) \cdot d\lambda} \cdot \frac{\int_{\lambda 1}^{\lambda 2} \ell_\lambda h_\lambda (2,870) \cdot d\lambda}{\int_{\lambda 1}^{\lambda 2} \ell_\lambda h_\lambda (B) \cdot d\lambda}$$

Utilizing the substitutions defined above:

$$\rho_{B0} = \frac{r_B/r_0}{\ell_B/\ell_0} = \frac{1}{\rho_{0B}} = \frac{\ell_0/\ell_B}{r_0/r_B} \qquad (8\text{-}25)$$

The actual output current produced by the different temperature background for the same visible luminance is not increased in this same ratio since the tube response may be non-linear. The effect of non-linear response on the output when viewing the sky background is analogous to a change in illumination from the 2,870°K calibration source by the factor, ρ_{B0}. A numerical study of the variation of ρ_{B0} with detector spectral sensitivity indicated that as long as the peak of the spectral response was in the visible at a wavelength longer than 0.50 μ, then the value of ρ_{B0} and the equivalent 2,870°K source illumination change implied, lie within the range of validity of Equation (8-17). Thus a different temperature background giving the same effective visual illumination gives a response satisfying:

$$I' = I + \Delta I$$

where:

$$\frac{\Delta I}{I} = \gamma \frac{\Delta B}{B}$$

B being the original luminance and ΔB the equivalent luminance increase.

Since image luminance and image illuminance differ only by a constant factor, we may write:*

$$L = \frac{BD^2 \theta^2}{4A} \qquad \Delta L = \Delta B \cdot \frac{D^2 \theta^2}{4A} \qquad (8\text{-}25')$$

Hence:

$$\Delta I/I_0 = \gamma \Delta L/L \qquad (8\text{-}26)$$

---

* The numerical factor results from the choice of units for D and θ. We retain the units ft^2 for A.

But:

$$\Delta L = (\rho_{B0} - 1)\, L; \quad \theta = \text{field-of-view angular subtent.} \tag{8-27}$$

Thus:

$$\Delta I = \gamma(\rho_{B0} - 1)\, I_0 \tag{8-28}$$

$$\therefore\ I' = [1 + \gamma(\rho_{B0} - 1)]\ I_0 \tag{8-29}$$

Now a derivation similar to that for Equation (8-21) will show that:

$$Q_R^0(B) = \frac{I'}{\eta LA} \left(\frac{\epsilon B}{e}\right)\left(\frac{hc}{\lambda}\right)\left[\frac{\int_{\lambda_1}^{\lambda_2} \ell_\lambda\, h_\lambda(B) \cdot d\lambda}{\int_{\lambda_3}^{\lambda_4} r_\lambda\, h_\lambda(B) \cdot d\lambda}\right]$$

Substituting from Equation (8-29):

$$Q_R^0(B) = \left[\frac{I_0}{\eta LA}\left(\frac{\epsilon_0}{e}\right)\left(\frac{hc}{\lambda}\right)\frac{\ell_0}{r_0}\right]\left(\frac{\ell B}{\ell_0}\right)\left(\frac{r_0}{rB}\right)\left(\frac{\epsilon B}{\epsilon_0}\right)\left[1 + \gamma\,(\rho_{B0} - 1)\right]$$

$$\therefore\ Q_R^0(B) = Q_R^0(2,870) \cdot \frac{\epsilon B}{\epsilon_0} \cdot \frac{1}{\rho B0} \cdot \left[1 + \gamma\,(\rho_{B0} - 1)\right]; \tag{8-30}$$

Q_R^0 (2, 870) being given by Equation (8-21).

For the tube whose transfer characteristic is shown in Figure 8-1, we found that:

$$\gamma \doteq 0.75 \text{ to } 0.80$$

Numerical evaluation of the integrals involved in Equation (9-12), using the spectral response curve for this tube and an empirical curve for the background spectral radiance, showed that:

$$\rho_{B0} \doteq 0.5$$

Finally, the integral r_B was compared to the integral

$$r_T = \int r_\lambda \cdot h_\lambda(T) \cdot d\lambda$$

for different values of T, indicating that the response to the background appeared very much like that to an 8, 000°K black body spectrum. The luminous efficiencies for black bodies may be determined to sufficient accuracy from published tables of black body chromaticity coordinates

and tables of maximum luminous efficiency for sources having such chromaticity coordinates (Reference 25). These yield values for the luminous efficiencies of:

$$\epsilon_B \doteq 385 \text{ lumens/watt, and; } \epsilon_0 \doteq 510 \text{ lumens/watt.}$$

Hence:

$$\frac{\epsilon_B}{\epsilon_0} \doteq 0.75 \tag{8-31}$$

Thus we find that, for this tube (the Machlett ML 7351), and with only a few percent error:

$$Q_R^0(B) \doteq Q_R^0(2,870) \tag{8-31'}$$

the approximation being in error by possibly 6 percent or less.

We thus conclude that for vidicons whose spectral sensitivity lies predominantly in the red portion of the visible spectrum, the photocathode responsive quantum efficiency when viewing daylight sky background is essentially the same as that when viewing a scene of the same illumination level, but illuminated by a black body source of temperature 2, 870°K.

Equation (8-21) shows that $Q_R^0(2,870)$ depends on I_0/L. If the image tube has nonlinear response ($\gamma \neq 1$) $Q_R^0(2,870)$ is not constant but dependent on photocathode illumination, L. Since the photocathode illumination is primarily by the background (a parameter which we wish to vary) it is necessary to eliminate Q_R from Equation (8-19). This may be accomplished by substituting Equations (8-13), (8-21), (8-21'), (8-24), (8-25), (8-25'), (8-30), and (8-31') into Equation (8-19) arriving at:

$$C_{m.th}^2 = \left(\frac{e\rho_{0B}\bar{\lambda}K_i^2\theta^2}{hc\gamma^2 R\epsilon_o a^2\tau}\right)\left(\frac{\tau}{\tau_0}\right)^{1-\gamma}\frac{1}{(\eta N_B)^{\gamma}} \tag{8-19''}$$

Without the approximation Equation (8-31'), this equation would be:

$$C_{m.th.}^2 = \left[\frac{}{1+\gamma(\rho_{B0}-1)}\right]\left(\frac{e\bar{\lambda}K_i^2\theta^2}{hc\gamma^2 R\epsilon_B a^2\tau}\right)\left(\frac{\tau}{\tau_0}\right)^{1-\gamma}\frac{1}{(\eta N_B)^{\gamma}} \tag{8-19'''}$$

We should point out that the spectral sensitivity of the ML 7351 vidicon peaks between 0.60 μ and 0.64 μ. Other types of vidicons, whose sensitivity peaked from 0.40 μ to 0.50 μ, were investigated. For these vidicons it was found that, because the background spectrum peaks very sharply between 0.45 μ and 0.50 μ, the value of ρ_{B0} varied between 0.70 and 0.10. This has the effect of reducing $Q_R(B)$ by as much as a factor of two. Thus,

for such vidicons the approximation Equation (8-31') for $Q_R(B)$ does not hold. However the values of measured contrast may be computed from Equation (8-19''') in this case.

8.5.2 Calculation of Effective Star Image Size, a

The characteristic Equation (8-19') and its companion Equation (8-20') contain the star image size parameter, a. In the derivation of these equations, the image was assumed to be a uniformly bright square, whereas the actual star image will be anything but this. It will thus be necessary to relate this "square" star image size to a physically more meaningful parameter, in particular, the star image half-width. Then Equations (8-19') and (8-20') may be written in terms of this parameter.

The effective square image size and the star image half-width may be related, once the intensity distribution in the image is known, by demanding that the total received power in the uniform square and in the real star image be the same, regardless of which parameter is used. Thus we may write:

$$a^2 f^2 H_S = a^2 a_{1/2}^2 f^2 H_S \qquad (8\text{-}33)$$

where a and H_S are as previously defined and:

f = focal length of optical system

$a_{1/2}$ = half-width of real star image

a = a constant

Thus:

$$a^2 = a^2 a_{1/2}^2 \qquad (8\text{-}34)$$

Suppose now that the relative intensity distribution in the image is $g(a_{1/2}, x, y)$, and that the intensity at the center of the actual image, and that at the center of the equivalent square image are the same. Then:

$$f^2 a^2 H_S = f^2 a_{1/2}^2 \iint g(a_{1/2}, x, y)\, dx \cdot dy \cdot H_S \qquad (8\text{-}35)$$

$$\therefore\ a^2 = \iint g(a_{1/2}, x, y) \cdot dx \cdot dy \qquad (8\text{-}36)$$

The intensity distribution in the star image is rather difficult to describe analytically. If starlight were monochromatic and if the image were perfectly stationary, the intensity would follow the well known distribution

$\left[J_1(x)/x\right]^2$, J_1 being the Bessel function of the first kind and of order 1, and x being the angular distance from the image center, expressed in an appropriate set of units. But the effects of atmospheric shimmer and the presence of a rather broad spectrum of wavelengths in starlight tend to distort this distribution.

Schade (Reference 26) has made an extensive study of point image definition and has evaluated the effect of various image intensity distributions on image definition. He has pointed out that a succession of aperturing processes seems always to cause the final image intensity to tend toward a Gaussian distribution. He has also pointed out that for an imaging process involving a series of apertures each having a Gaussian aperture transmittance (and thus Gaussian sine wave response functions) the overall system sine wave response function is Gaussian. Finally, his numerical calculations with different apertures have shown that round apertures with $\cos^2$ and Gaussian transmittance functions have essentially the same aperture response. This indicates that any symmetric, round aperture transmittance function having a smoothly varying transmittance over the central area of the aperture but falling off exponentially from the aperture center, will have essentially the same response function.

Now the imaging process involved in a daylight startracker involves at least three aperturing processes (optical aperture, electron scanning-beam aperture, and electronic signal-processing filter aperture). Schade's work thus indicates that little accuracy wil be lost, in our analysis of overall system response, if the optical image is assumed to have a Gaussian intensity distribution. We may thus write, for the approximate star image intensity distribution:

$$g(a_{1/2}, x, y) = e^{-\frac{4b^2x^2}{a_{1/2}^2}} \cdot e^{-\frac{4b^2y^2}{a_{1/2}^2}} \qquad (8\text{-}37)$$

where:

$b = 0.693$

$a_{1/2}$ = star image half-width

x, y = orthogonal angular coordinates (e.g. azimuth and elevation) relative to the image center

Hence:

$$a^2 \doteq \iint_{\text{image}} g(a_{1/2},\, x,\, y)\, dx \cdot dy \doteq 2\int_0^\infty e^{-\frac{b^2x^2}{a_{1/2}^2}} \cdot dx \cdot 2\int_0^\infty e^{-\frac{b^2y^2}{a_{1/2}^2}} \cdot dy$$

$$= \left[2\int_0^\infty e^{-\frac{b^2u^2}{a_{1/2}^2}} \cdot du\right]^2 = \left[2\,\frac{a_{1/2}}{2b}\left(\frac{\sqrt{\pi}}{2}\right)\right]^2$$

$$= \frac{\pi a_{1/2}^2}{4b^2} = 1.64\, a_{1/2}^2$$

or:

$$a = 1.28\, a_{1/2} \qquad (8\text{-}38)$$

In words, Equation (8-38) states that the equivalent, uniform square image has an edge length 1.28 times the real star image half-width, assuming the image intensity distribution is Gaussian. The equivalent square image and the real image have the same illuminance at their image centers.

We may now complete our modification of the characteristic Equation (8-19'') and its companion Equation (8-20'), by replacing a by $1.28\, a_{1/2}$. That is:

$$C_{m.th}^2 = 0.61G \left(\frac{e}{hc}\right)\left(\frac{\rho_{0B}\bar{\lambda}}{\gamma^2 R\epsilon_o}\right)\left(\frac{1}{\tau_o}\right)^{1-\gamma}\left(\frac{K_i^2\,\theta^2}{a_{1/2}^2}\right)\left(\frac{1}{\eta N_B \tau}\right)^{\gamma} \qquad (8\text{-}39)$$

$$C_{m.s.} = \frac{0.61\gamma\, H_S\, \rho_{TB}}{N_B\, a_{1/2}^2} \qquad (8\text{-}40)$$

For those detectors for which the approximation Equation (8-31') is not valid, we substitute Equation (8-38) into Equation (8-19''') to get:

$$C_{m.th}^2 = \left[\frac{0.61G}{1+\gamma(\rho_{B0}-1)}\right]\left(\frac{e\bar{\lambda}K_i^2\,\theta^2}{hc\gamma^2 R\epsilon_B a_{1/2}^2 \tau}\right)\left(\frac{\tau}{\tau_0}\right)^{1-\gamma}\left(\frac{1}{\eta N_B}\right)^{\gamma} \qquad (8\text{-}39')$$

These equations are not restricted in validity to television image tubes only. They are valid for any image-forming photosensor providing the following restrictions are met:

1. The detector may have linear or nonlinear response:

   a) If the detector response is linear, there are no restrictions;

   b) If the detector response is nonlinear then the response must obey Equation (8-13).

2. The scene contrast (star image luminance/sky background luminance is:

   a) Unrestricted for linear detectors;

   b) Restricted to low-, to medium-contrast for detectors with nonlinear response, the upper contrast limit depending on the degree of nonlinearity (the parameter γ in Equation (8-13).

3. The detector spectral response must peak in the near ultraviolet, visible or near infrared, and should have a spectral bandpass of about 2,000 Å to 3,000 Å.

   a) If the detector has relatively little response below 5,000 Å, then Equation (8-39) should be used.

   b) If the detector has appreciable response (50 percent or more) around 5,000 Å or below, then Equation (8-39') should be used.

4. The image spot at the photocathode must have approximately a Gaussian intensity distribution.

5. The quantity τ has the following meaning:

   a) For detectors possessing memory, τ is the exposure time.

   b) For detectors without memory, τ is the time constant of the readout circuitry.

Section 9

EVALUATION OF PRACTICAL IMAGE TUBE LIMITATIONS ON STARTRACKER PERFORMANCE

As mentioned previously in subsection 8.5, the performance of a daylight startracker having a quasi-ideal, memory-possessing, image tube may be determined with the aid of Equations (8-39) and (8-40). Having chosen the system configuration and the photosenosr, all the parameters in Equations (8-39) and (8-40) except ρ_{TB}, H_s, and N_B, and $a_{1/2}$ are determined. One then establishes several values of background radiance, N_B, of star illuminance, H_S, and of star temperature*, T, witnin the ranges of interest. Then the value of the measured contrast at detection threshold, $C_{m.th}$, may be determined from Equation (8-39) as a function of $(\frac{1}{a_{1/2}})$. Once all parameters (including N_B) are determined, we see from Equation (8-39) that:

$$C_{m.th} \sim \frac{1}{a_{1/2}}$$

Hence, on a log $(C_{m.th})$ versus log $(\frac{1}{a_{1/2}})$ plot, the locus of Equation (8-39) for the chosen value of N_B is a straight line of slope 1. Thus the loci of Equation (8-39) on such a graph, corresponding to the chosen set of background radiance values, N_B, will be a family of parallel, straight lines, having unit slope. Similarly, the loci, Equation (8-40) will be a family of parallel, straight lines, having slope two. These curves, displayed on the log C_m versus log $\frac{1}{a_{1/2}}$ graph, will be referred to as the "system Performance chart".

A typical system performance chart is shown in Figure 9-1. System parameters for the chart are discussed in detail in subsection 9.9. Subsections 9.2 through 9.8 discuss the manner of incorporating various system parameters into the chart.

In previous discussions we have established that:

(1) For image tubes viewing a bright background, photocathode imperfections and mesh-image may limit the minimum contrast detectable (Section 7.9).

---

* The navigational stars range in temperature from about 3,000°K to 20,000°K.

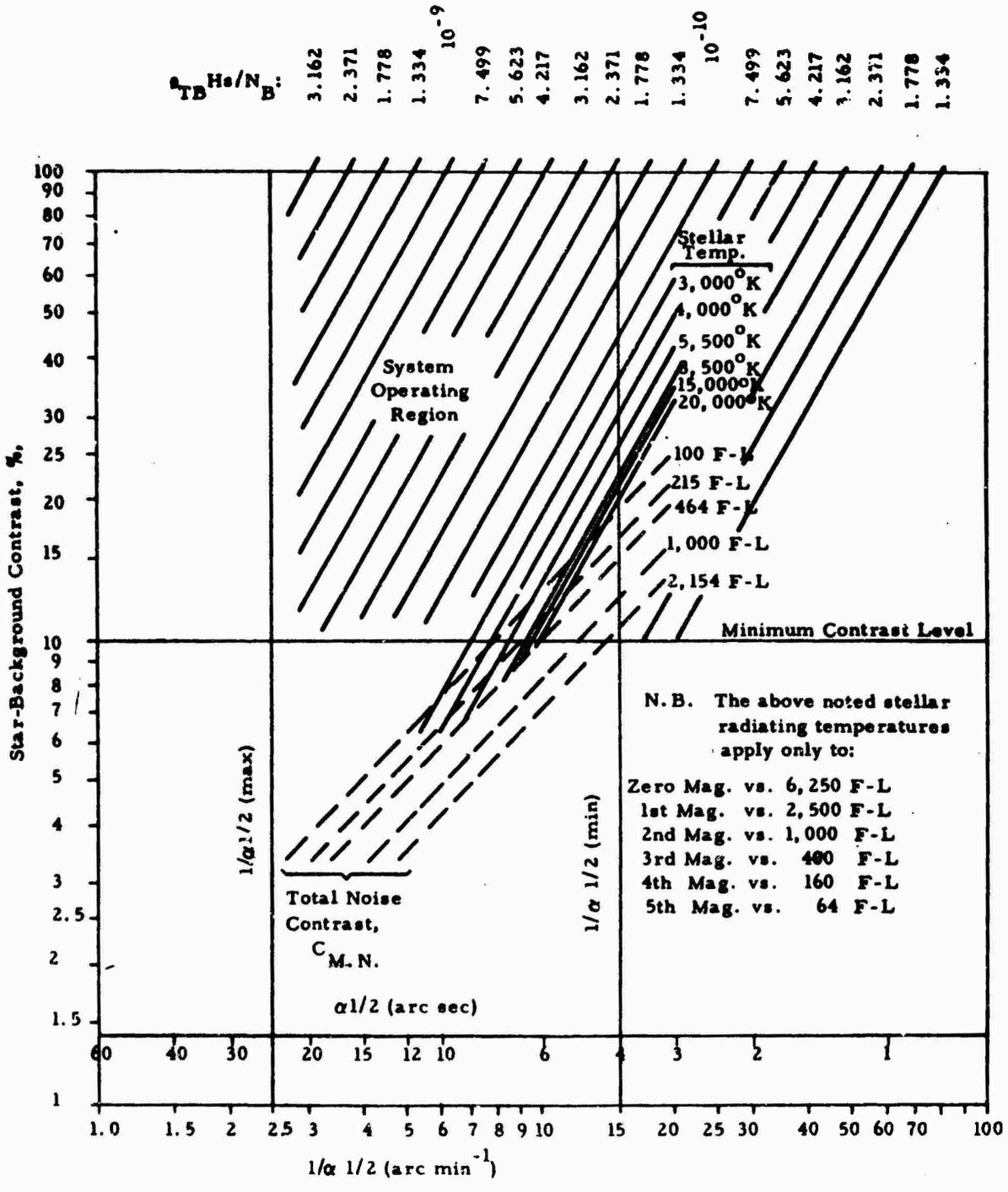

FIGURE 9-1 SYSTEM PERFORMANCE CHART (See also Table 3)

Performance of a daylight star tracker operating in a "shuttered" mode with a Machlett ML7351 Vidicon.
Exposure: 1/90 sec; readout: 1/30 sec.

N.B 1 foot-lambert = 1.58×10^{-6} watts/cm^2 ster.

π ft-candle = π ft-lambert = 1 lumen ster^{-1} ft^{-2}

(2) Electronic noise is independent of photocathode illumination and depends on readout electronic bandwidth (Section 7.4).

(3) There is a lower limit to the minimum size of electron read-out beam available in contemporary image tubes (Section 7.9).

Finally, we should take cognizance of three additional factors which will decrease or increase the amplitude of the detected star signal. These are:

(4) Amplitude decrease due to atmospheric scintillation, and

(5) Amplitude decrease due to the raster-scanning method used in image tubes,

(6) Amplitude increase or decrease due to dependence of actual tube response on star-effective temperature, for a star of a given effective visual magnitude.

We shall now discuss the manner in which each one of these practical limitations may be incorporated into the system performance chart.

9.1 PHOTOCATHODE IMPERFECTIONS AND MESH IMAGE LIMITATIONS

It is quite obvious from the discussion in subsection 7.9 that photocathode imperfections and mesh image produce false image detail in a uniform scene which is directly proportional to the scene brightness. Thus, these details may be considered as "detector-scan noise", whose contrast with respect to the background is fixed. If we assume that there is a maximum amplitude for this contrast (considering only those details having Fourier components within the bandpass of the electronic readout circuitry) then this represents a minimum contrast for a detectable star image. We thus draw a line across the system performance chart at this minimum contrast value, and demand that the system perform only in that region above this line.

NASA's specification for the TIROS vidicon* (Reference 22) make it obvious that the minimum contrast set by tube imperfections is a function of the size of the imperfection. This function will be dependent on the electronic bandwidth and on the position of the center frequency within the pass band. For lack of more precise knowledge we will have to assume this line to be of constant contrast, independent of any size parameter. Thus the minimum contrast line on Figure 9-1 will be horizontal, and the system must operate above it.

---

* See also the last paragraph of subsection 7.9.

9.2 ELECTRONIC NOISE LIMITATIONS

Noise current in the photosensor electronic readout circuitry can be related to the electronic bandwidth and other system parameters, such as image size, frame rate, etc., and also to the noise data supplied by image tube manufacturers. The operating current as a function of background illumination level is also easily established. The dependence of electronic noise contrast on $\alpha_{1/2}$ may then be derived.

9.2.1 Relating Noise Current, Readout Time, Image Size, and Tube Noise Data

Assume that the electronic readout system reads out the entire image in a period τ' (not necessarily equal to the image exposure time, τ). Then the electronic bandwidth required is:

$$\Delta f = \frac{mM^2}{2} \tag{9-1}$$

with

$$m = \frac{1}{\tau'} = \text{readout frame rate} \tag{9-2}$$

$$M^2 = \frac{\Omega}{\alpha_{1/2}} \tag{9-3}$$

$$\Omega = \theta^2 = \text{field-of-view solid angle} \tag{9-4}$$

$$\therefore \Delta f = \frac{\theta^2}{2\alpha_{1/2}^2 \tau'} \tag{9-5}$$

Now the usual data available on electronic noise in image tubes concerns that in a standard video bandwidth of five megacycles/second, which is sufficient to sample 10 resolution elements per second. This is equivalent to a 525 line raster, resolving 630 vertical lines, at 30 frames per second. Let i_{no} be the rms electronic noise current in this standard video band pass, and i_n be that in the startracker circuitry, with bandpass Δf. Then, assuming noise current is proportional to the square root of the bandwidth:

$$\frac{i_n}{i_{no}} = \sqrt{\frac{\Delta f}{5 \times 10^6}} = \frac{10^{-4}\theta}{\alpha_{1/2}} \sqrt{\frac{10}{\tau'}} \tag{9-6}$$

Note that:

$$\frac{i_n}{i_{no}} = \frac{K_i\ i_n}{K_i\ i_{no}} \qquad (9\text{-}7)$$

Here $K_i\ i_n$, and $K_i\ i_{no}$ represent the threshold detection currents for the startracker bandwidth and the standard video bandwidth respectively. Note also that i_n/i_{no} is a linear function of $\frac{1}{a_{1/2}}$

By setting $i_n = i_{no}$ in Equation (9-5), we may find $a_{1/2}$ for the case where the startracker bandwidth is 5 Mc/s.

$$a_{1/2}\ (\text{Ref.}) = 10^{-4}\ \theta\ \sqrt{\frac{10}{\tau'}} \qquad (9\text{-}8)$$

9.2.2 Determining Background Current, I', and Noise Current i_{no}

Suppose that we have chosen τ', θ , and $a_{1/2}$ such that $i_n = i_{no}$. (We assume the rms noise current in the startracker electronics pre-amplifier is the same as that reported by the manufacturer.) We may then utilize the tube transfer characteristics, noise current data, and background spectral radiance data to determine both the output current, I', resulting from the scanning of the background, and an "equivalent background noise source" giving an output current $K_i\ i_n$, and thus establishing an electronic noise contrast $Ce = \frac{K_i\ i_n}{I'}$

The effective visual illumination of the tube by the background, L , is given by Equation (8-5') as:*

$$L = \frac{N_B D^2\ \theta^2}{4A} \qquad (9\text{-}9)$$

Equation 9-10 omitted.

Tube response current I', for this background illumination, differs from the response to a 2,870°K calibration source, I, having the same effective visible illumination.

* We identify the symbol Δ of Equation (8-25') with N_B. Cf. also the remark following Equation 8-18 of Paragraph 8.4.1. The units for A are ft^2.

Symbolically we may write this as:

$$I'(B) = I'(\rho_{B0} L)$$

The parentheses indicate functional dependence of their contents on the preceding symbol.

The tube responds as if it were being illuminated by a 2,870°K source of illuminance L' given by

$$L' = \rho_{B0} L \tag{9-11}$$

In paragraph 8.5.1 we established (Equation 8-29) that:

$$I'(B) = \left[1 + \gamma (\rho_{B0} - 1)\right] \cdot I'(2870) \tag{9-12}$$

The noise current, i_{no}, may be calculated for image orthicons directly from the manufacturer's published signal current and signal-to-noise ratio. For vidicons, the signal-to-noise ratio is almost universally 100 at a signal current of 0.2 microamperes, giving a noise current $i_{no} = 2 \times 10^{-9}$ amperes.

9.2.3 Incorporating Electronic Noise Into the System Performance Chart

The ratio of the detection threshold current, $K_i i_n$, to the background signal current I, is the electronic noise contrast, C_e. That is:

$$C_e = \frac{K_i i_n}{I'} \tag{9-13}$$

Substituting (8-21h), (9-6) and (9-12) into (9-13):

$$C_e = \frac{K_i i_{no} \times 4.47 \times 10^{-4} (\tau')^{1/2}}{\left[1 + \gamma (\rho_{B0} - 1)\right] \cdot I_o \cdot \tau_o} \left(\frac{\tau_o}{\tau}\right)^{\gamma} \frac{\theta}{\alpha_{1/2}} \tag{9-14}$$

(Equations 9-15, 9-16, and 9-17 are omitted.)

Substituting (8-13) into (9-14) we get:*

$$C_e = \frac{4.47 \times 10^{-4} K_i i_{no} \theta (\tau')^{1/2}}{R \cdot \left[1 + \gamma(\rho_{BO} - 1)\right] \cdot \alpha_{1/2} \tau_o} \left(\frac{\tau_o}{\tau}\right)^{\gamma} \left(\frac{1}{\eta N_B}\right)^{\gamma} \quad ** \tag{9-18}$$

* Note that the quantity B in Equation (8-13) must be replaced by the effective photocathode luminance.

** A plot of Equation (9-18) for various values of N_B and for $i_{no} = 2 \times 10^{-9}$ amperes is given in Figure 9-3.

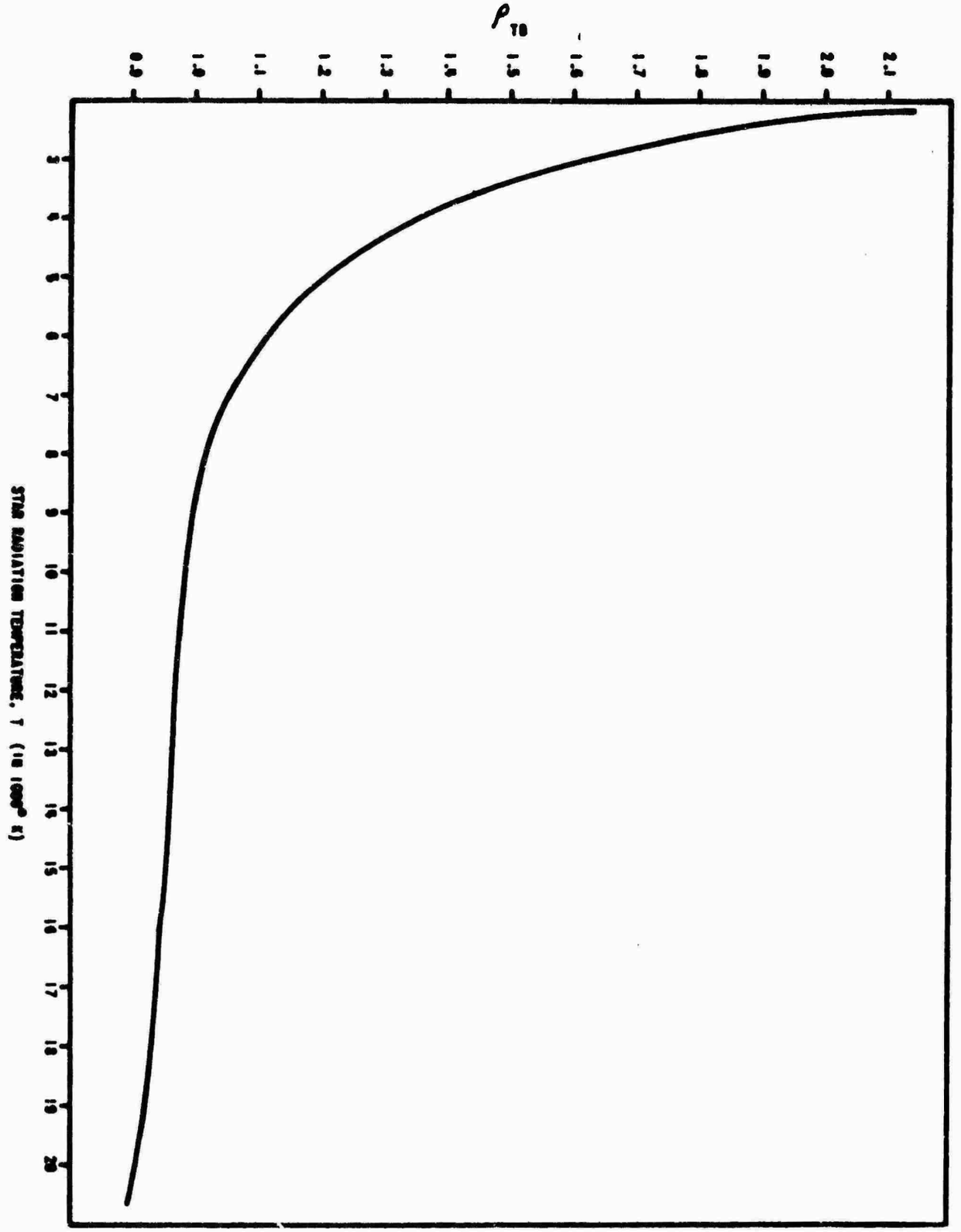
ρ_{TB}

Electronic noise will degrade startracker performance whenever the electronic noise contrast, C_e, Equation (9-10) exceeds measured star/background contrast, $C_{m.s.}$ Equation (8-40), that is, whenever:

$$C_e \geq C_{m.s.}$$

We may incorporate this limit into the system performance chart in the following way. Substitute into Equation (9-18) the maximum value of N_B against which the system must be operated and plot the locus of C_e versus $1/a_{1/2}$. The system must operate in the region above this line.

Electronic noise will dominate over background photon noise if the electronic noise contrast, as given by Equation (9-18), exceeds the measured contrast at detection threshold, C_{mth}. Thus we must require:

$$C_{mth}(N_B) \leq C_e(N_B) \tag{9-19}$$

Substituting Equations (8-25), (8-39), and (9-18) into this gives:

$$\left[\frac{1.91 \times 10^{-17} e\,\bar{\lambda}\,\rho_{OB} K_i^2\,\theta^2}{(\eta N_B)^{\gamma} hc\,\gamma^2\,\epsilon_o\,R\,a_{1/2}^2\,\tau}\left(\frac{\tau}{\tau_o}\right)^{1-\gamma}\right]^{1/2} \leq \frac{4.47 \times 10^{-4} K_i\, i_{no}\,\theta\,(\tau')^{1/2}(\tau_o/\tau)^{\gamma}}{R\cdot\left[1+\gamma(\rho_{BO}-1)\right]^{\gamma} a_{1/2}\,\tau_o\,(\eta N_B^{\gamma})} \tag{9-20}$$

$$\therefore N_B \leq \left[\frac{1.046 \times 10^{12}\, i_{no}^2\, hc\,\gamma^2\,\epsilon_o\,\rho_{BO}\,\tau'^2}{R\,\eta^{\gamma}\,e\,\bar{\lambda}}\right]^{1/\gamma} \frac{\tau_o}{\tau\left[1+\gamma(\rho_{BO}-1)\right]^2} \tag{9-21}$$

Thus there is a value, N_B', such that:

$$C_{m.th}(N_B') = C_e(N_B') \tag{9-19'}$$

Note from (9-21) that N_B' depends only on photosensor parameters and the spectral radiance of the sky background; it is independent of the other system parameters.

If the actual background luminance, N_B, is less than N_B', electronic noise is dominant, while if N_B is greater than N_B' background photon noise predominates. The example to be discussed in subsection 9.9 is one in which electronic noise predominates. Whenever background photon noise dominates, the photosensor is operating as a quasi-ideal detector.

These two noise sources, being uncorrelated can be combined to yield the total measured noise contrast $C_{m.n.}$ (exclusive of detector-scan noise) by taking their root squared sums (rss). Thus, utilizing Equations (8-39) and (9-18) we get:

$$C_{m.n.} = \left\{ \left(\frac{1.91 \cdot 10^{-10} e \bar{\lambda}}{\rho_{BO} hc \gamma^2 \epsilon_o \tau} + \frac{2 i_{no}^2 \tau' (\tau/\tau_o)^{1-\gamma}}{R\left[1+\gamma(\rho_{BO}-1)\right]^2 \tau^2 (\eta N_B)^\gamma} \right) \left[\frac{10^{-7} K_i^2 \theta^2}{R a_{1/2}^2 (\eta N_B)^\gamma} \left(\frac{\tau}{\tau_o} \right)^{1-\gamma} \right] \right\}^{1/2} ; \quad (9\text{-}18')$$

For those detectors for which Equation (8-39'), rather than (8-39) is valid, $C_{m.n.}$ is given by:

$$C_{m.n.} = \left\{ \left(\frac{1.91 \times 10^{-10} e \bar{\lambda}}{hc\gamma^2 \epsilon_B \tau} + \frac{2 i_{no}^2 \tau' (\tau/\tau_o)^{1-\gamma}}{R\left[1+\gamma(\rho_{BO}-1)\right] \tau^2 (\eta N_B)^\gamma} \right) \left[\frac{10^{-7} K_i^2 \theta^2 (\tau/\tau_o)^{1-\gamma}}{R\left[1+\gamma(\rho_{BO}-1)\right] a_{1/2}^2 (\eta N_B)^\gamma} \right] \right\}^{1/2} \quad (9\text{-}18'')$$

Equations (8-40), and (9-18')* together represent the mathematical model by means of which the performance of a wide field-of-view daylight star tracker employing almost any image-forming photosensor may be evaluated.

An upper limit for the background luminance may be obtained once the dimmest star of interest to the system is specified. One requires that the star/sky contrast be greater than the threshold contrast. That is:

$$C_{m.s.} \geq C_{m.th.} \quad (9\text{-}22)$$

---

*or 9.18", as the case may be

Substituting Equations (8-39) and (8-40):

$$\frac{\gamma^2 H_s^2 \rho_{TB}^2}{2.66^2 \times 10^{-16} N_B^2 a_{1/2}^4} \geq \frac{1.91 \times 10^{-17} e \bar{\lambda} \rho_{OB} K_i^2 \theta^2 (\tau/\tau_o)^{1-\gamma}}{hc \gamma^2 R \epsilon_o a_{1/2}^2 \tau (\eta N_B)^\gamma} \quad (9\text{-}23)$$

$$\therefore \left[\left(\frac{\tau_o}{\tau}\right)^{1-\gamma} \frac{hc \gamma^4 R \epsilon_o \eta^\gamma \rho_{TB}^2 \rho_{OB} \tau H_s^2}{1.35 \times 10^{-32} a_{1/2}^2 e \bar{\lambda} K_i^2 \theta^2}\right]^{\frac{1}{2-\gamma}} \geq N_B \quad (9\text{-}24)$$

The maximum value, N_{Bmax}, can be calculated from Equation (9-24) once one specifies the dimmest star illuminance, H_{Smin}, and a value for the image half-width. An oblique line establishing the lower limit for the system operating region on the system performance chart may thus be drawn. The system then is restricted to operating above this line. Thus, the lower boundary of the system operating region is determined either by this line, by the electronic noise line, or by the minimum contrast line determined by photocathode imperfections, whichever is greater (See Figure 9-1).

9.3 MINIMUM ELECTRON BEAM SIZE LIMITATIONS

For optimum performance, the electron beam half-width should be matched to the star image half-width, $a_{1/2}$. The state of the art in electron beam focussing in image tubes is such that the minimum electron beam half-width is just slightly less than 0.5×10^{-3} inch.

The above two statements imply that, on the system performance chart, the region to the right of the maximum value of $1/a_{1/2}$, corresponding to the minimum electron beam half-width, is not accessible to the system.

9.4 STAR SCINTILLATION LIMITATIONS

For two to four inch optical apertures, scintillation causes star signal amplitudes to vary by as much as 35 percent. This may be taken into account merely by using a reduced value of effective stellar illumination when evaluating performance with the system performance chart. The reduced value will depend on the actual method of system operation and need not be quite as severe as 35 percent. Subsection 9.7 discusses a method of operation in which this is true.

9.5 STAR SIGNAL-AMPLITUDE REDUCTION FROM RASTER-SCANNING

The electron beam center will not generally scan directly across the star image center. Thus, star signal amplitude could vary between the maximum, for a direct "hit" by the scanning beam, and a minimum, occuring when the image lies midway between raster lines. This may be accounted for in the same manner as described in subsection 9.3. For the present it will be assumed that the difference between maximum and minimum signal is negligible, and no attempt will be made to determine the actual difference.

9.6 AMPLITUDE CHANGES FROM DIFFERENCES IN EFFECTIVE STELLAR RADIATION TEMPERATURES

This is accounted for by the factor ρ_{TB} introduced into (8-20') in paragraph 8.4.2. The reduction factor for stars of a given effective visible illumination varies as to their effective irradiance, due to differences in effective stellar radiating temperatures (See Figure 9-3). However, for detectors sensitive in the visible and near IR this irradiance variation between cold and hot stars of the same visual magnitude is approximately a factor of two. Thus each illumination value calculated from Equation (8-39) corresponding to a particular threshold contrast, does not represent a unique value of visual stellar magnitude. If the visual magnitude is calculated by the usual formula (without color, or bolometric correction factors),

$$m_s = 2.5 \log_{10} \frac{H_{s,\min}}{H_o} \qquad (9\text{-}25)$$

It will represent the magnitude of an AO class star only.

Here H_o represents the illumination from an AO class star of zero magnitude. Its value is:

$$H_o = 3.1 \times 10^{-13} \text{ watts/cm}^2$$

Stars of other classes giving the same effective irradiance, will have a visual magnitude falling between the magnitude calculated from Equation (9-25) and a value of 0.56 magnitude brighter. Thus, a true minimum visible stellar magnitude for a given minimum irradiance may be calculated from:

$$m_{s,\min} = 2.5 \log \left(\frac{H_s}{H_o} \right) - 0.56 \qquad (9\text{-}26)$$

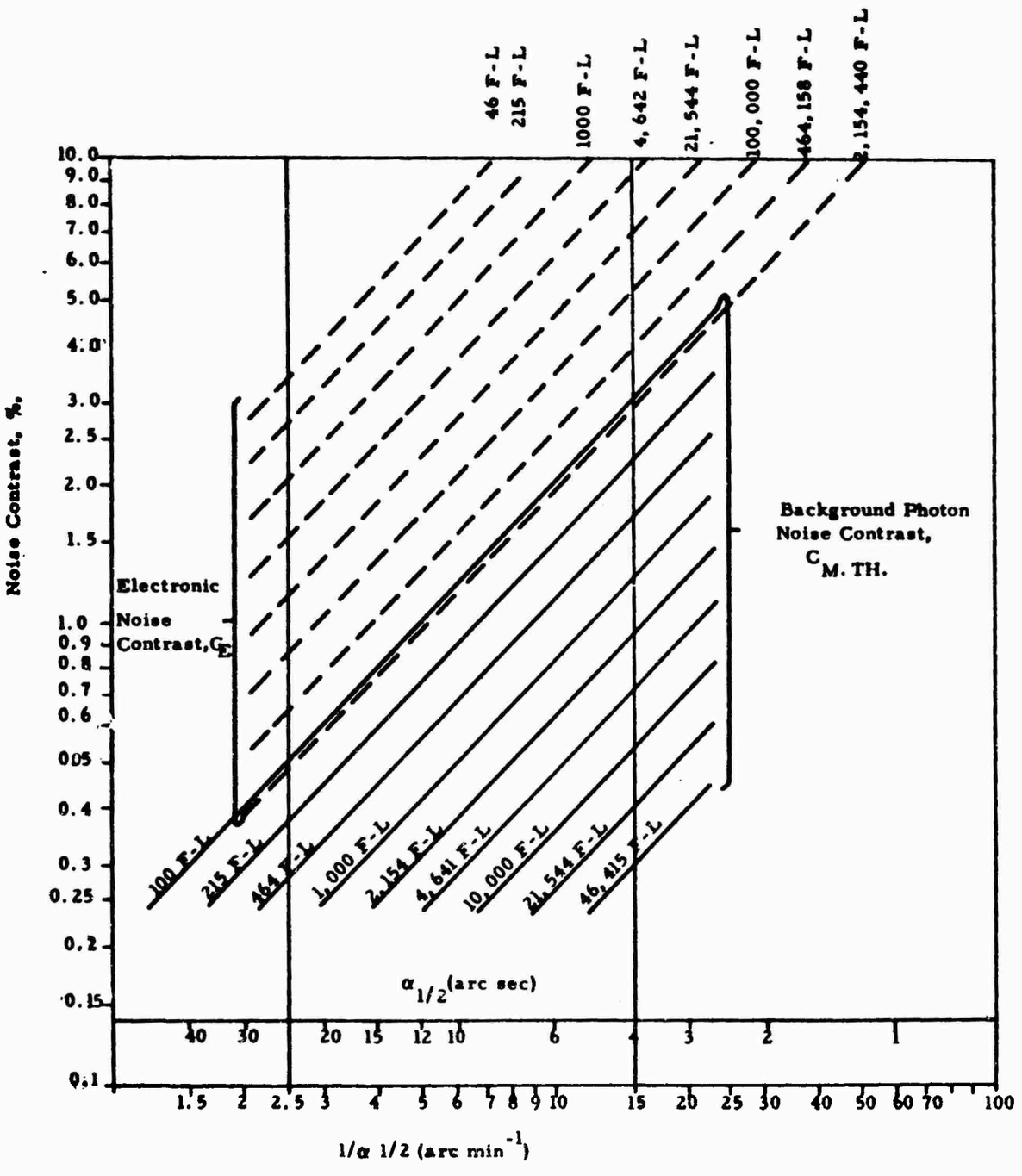

FIGURE 9-3. SYSTEM AND BACKGROUND NOISE 23:

Daylight star tracker operating in shuttered mode. (See also Table 3)

N.B. 1 ft-lambert $\doteq 1.58 \times 10^{-6}$ watts/cm^2 ster.

9.7 STAR/SKY CONTRAST ENHANCEMENT BY POLARIZERS

The star signal reductions due to the phenomena discussed in subsections (9.5) and (9.6) may be partially, if not completely, offset by the use of polarizing filters. Indeed, the contrast may be made greater than before these reductions were considered. The technique utilizes the well-known fact that Rayleigh-scattered sunlight from the atmosphere is partially polarized, whereas direct starlight is not. Thus, the neglect of the reduction factors in the analysis is entirely reasonable.

9.8 "SHUTTERED" OPERATION OF AN IMAGE TUBE AND REDUCTION OF IMAGE PERTURBATIONS

The discussions of Section two point up the fact that, if the photosensor exposure time, τ, is long enough ($\gtrsim$ 1/30 second) atmospheric shimmer would smear the star image to twice its diffraction-limited size, while servo loop transients even in a high-precision stabilized platform, might quadruple it. Thus a high-contrast, diffraction-limited image of about 100 percent contrast could be reduced, through such image perturbations, to a low contrast of about 6 percent.

These perturbations can be eliminated by exposing the image for a brief exposure of about 5 to 10 milliseconds or so. This effectively "stops" the dancing motion of the image, since platform transient and atmospheric shimmer oscillation amplitudes at around 200 cps are very small compared to those in the 5 to 60 cps range. One must be careful not to expose the scene for too short a period as this increases the background photon noise relative to the signal and thus increases the threshold contrast, $|C_{m.th}|$.

Such "shuttered" operation can be performed with a mechanical shutter, and may possibly be accomplished electronically. The image may then be read out in normal fashion (30 frames/second) or at a slower rate, if desired. The slower the readout, the lower will be the electronic noise contrast, C_e. (See Equation 9-18).

With this scheme, instead of a perturbation-smeared image several times the diffraction-image size, one gets a sharply-defined, diffraction-limited (or nearly so) image, displaced by as much as several star image diameters from where it should be. It is thus apparent that to achieve an accuracy comparable to the size of the image, one must read several image positions and average them. For example, if stellar motion from all causes had a standard deviation of six arc-seconds, six observations would reduce the error to 2.45 arc-seconds. If readout were done at 30 frames/second, five such accurate fixes could be made per second.

Table 3 below, lists the mode of operation, photosensor, and other parameters used to compute the system performance chart, Figure 9-1.

TABLE 3. SYSTEM AND PHOTOSENSOR PARAMETERS FOR THE SYSTEM PERFORMANCE CHART (See Figure 9-1)

1. System Parameters		
a) Operational mode	sheltered	
b) Time constants	exposure time (t_e)	1/30 sec
	readout time (t_r)	0.0333 sec
c) Optical system	diameter (D)	2.0 inches
(almost diffraction-limited)	transmittance (τ_o)	0.5
	field-of-view (f.o.)	1.0 deg x 1.0 deg
	image size (typical, $\sigma_{I/2}$)	~0.10 arc minute
	(a min. a max)	(0.05, 0.30 arc minutes)
d) minimum signal-to-noise ratio		6.0
2. Radiation parameters		
a) Background, max. tolerable (W_B):		~1,000 ft - lamberts
b) Stellar min. illuminance (W_{SM}): (2nd magnitude star, visual)		2.0×10^{-13} watts/cm^2
c) Stellar radiating temperatures		3,000°K - 30,000°K
3. Photosensor parameters (Hamilton RCA-7265 vidicon)		
a) photocathode:		
size		1/2 in x 1/2 in
background illumination		6.30 ft-candle
stellar illumination (at image center)		0.11 ft-candle
screen contrast (photopic)		0.365
responsivity (R)		2.414×10^{-9} amperes/ft-lambert
Q_{PE} (2870) at 0.001 ft-c, 1/30 sec exposure		0.407 elec/photon
transfer characteristic slope (γ)		0.75
luminous efficiency viewing background relative to that for 2,870°K source temp. (ϵ_B/ϵ_O)		0.75
response when viewing background relative to that for 2,870°K source temp. (ρ_{BO})		0.80
minimum contrast detectable		=10 percent (for all $\sigma_{I/2}$)
b) electronics		
beam half-width ($\sigma_{I/2}$)		0.83×10^{-3} in.
bandwidth (Δf)		5.4 Mc/s
rms electronic noise current (i_n)		2.00×10^{-9} amp
rms electronic noise current (i_{no}) (reference)		2×10^{-9} amp
bandwidth (reference)		5 Mc/s
background current		0.151×10^{-6} amperes
star signal current		0.0175×10^{-6} amperes (2nd mag., 0.500 ft star)
electronic (measured) contrast (C_m)		11.5 percent
electronic signal-to-noise ratio		6.30
electronic image contrast		8.1% at $\sigma_{I/2}$ 0.1 min, N_H = 1,000 ft-l
image contrast (background and electronic)		8.2% at $\sigma_{I/2}$ 0.1 min, N_H 1,000 ft-l

These parameters suffice to allow plotting on the system performance chart (Figure 9-1) the loci of Equations (9-18') and (8-40) for various values of H_s and N_B. A locus of (8-39) is for a fixed value of N_B;* while a locus of (8-40) represents constant value of H_s/N_B. Equations (9-18), (9-18') and (9-21) were employed with a minimum required star illuminance from a second magnitude star, and maximum background of 1,000 foot-lamberts. These established the upper and lower limits to the system operating region due to electronic noise and sky background photon noise. Vertical lines were drawn representing the minimum electron beam half-width (about 0.43×10^{-3} inch, or three arc-seconds) and the maximum allowable image size (set by required system accuracy at about 30 arc-seconds). Finally, the line representing the minimum contrast limit set by image tube imperfections, was drawn at a conservative 10 percent.

The use of the system performance chart for a given photosensor is fairly simple. One selects values for stellar illuminance, H_s, and background luminance N_B, within the ranges of interest and computes the corresponding values of $\rho_{TB}/H_S/N_B$. Figure 9-2 gives a graph of the approximate value of ρ_{TB} versus star temperature, τ, for this purpose. Then, going to the locus of Equation (8-40) for this value, one sees whether or not the star/background contrast, C_s passes through the system operating region on the chart (the solid lines in Figure 9-1 are labeled by star radiation temperatures). In Figure 9-1 this occurs for image sizes, $a_{1/2}$, smaller than 10 arc-seconds. Next, the locus of Equation (8-39) for the chosen value of N_B is examined to see whether the star/background contrast exceeds the measured threshold contrast, $C_{m.th}$ established by the background photon noise. Now, the electronic noise contrast, C_e, for the brightest background against which the system must operate, may be computed from Equation (9-18') and plotted on the system performance chart; this reveals whether or not the electronic noise contrast, C_e is greater than measured star/background contrast, $C_{m.s.}$, and also whether electronic noise or background photon noise predominates in the system. Finally the noise contrast due to the two combined sources may be calculated from Equation (9-18') for the maximum background and plotted.

* See Figure 9-3 for a plot of the measured threshold contrast for various sky luminances.

Section 10

CONCLUSIONS

10.1 TUBE TYPES APPLICABLE

Limitations of size, weight, and sensitivity limit the use of image-forming photosensors in flight-worthy, daylight startrackers of all-altitude capability to the vidicon.

10.2 FEASIBILITY OF IMAGE TUBES FOR DAYLIGHT STARTRACKERS

The discussion and analysis of Sections 7, 8 and 9, and the calculation results of subsection 9.9 (presented in Figure 9-1) indicate the feasibility of daylight startrackers employing vidicons. Such trackers operating in a shuttered mode should be able to detect and track with contemporary vidicons stars of second magnitude against a background slightly brighter than 1,000 foot-lamberts. Star position readout is possible up to 30 or more times per second. System accuracy would depend on the number of star positions which are averaged. Averaging six positions would give readout at least five times per second with a standard error around three arc-seconds, while no averaging would give readout 30 or more times per second with a standard error of roughly 10 arc-seconds.

10.3 IMAGE TUBE LIMITATIONS OF DAYLIGHT STARTRACKERS

10.3.1 Image Size

It is important to note, from Figure 9-1, that the production of small-image size is important to the operation of the system from the standpoint of:

1. Overcoming electronic noise
2. Overcoming background photon noise, and
3. Overcoming minimum contrast restrictions.

It is thus apparent that minimum achievable image size is a practical limitation to the performance of the systems under consideration in this paper. Thus, any analysis such as the foregoing, based on a diffraction-

limited image, will give an upper limit to system performance. It appears also that manufacturing limitations limit the final image size through minimum electron readout beam size achievable.

10.3.2 Retina Imperfections

One serious limitation to the detection of stars dimmer than that indicated in Subsection 10.2 is the minimum contrast limitation imposed by photocathode imperfections, mesh image, etc. The severity of this problem, however, is not precisely known. Much more experimental data is needed to establish the contrast of tube-produced image irregularities as a function of the size of the irregularities. The type of data needed is essentially a Wiener spectrum of the image of a uniform scene.

It is highly desirable to reduce the tube-produced image irregularities (or detector-scan noise as we have called them previously). Methods of doing this are:

1. Refinement of the tube design and production so that image irregularities are eliminated or reduced to non-objectionable proportions. This is the preferred method.

2. Masking of the tube faceplate to compensate for the image detail. This was mentioned previously in Subsection 7.9.

3. The topic of "special processing of the output signal to reduce or eliminate tube irregularities" will be discussed at some length in Subsection 10.4.

Presently, it should be possible to procure image tubes with false image detail of star image size (approximately 0.5 to 1.5 by 10^{-3} inches) not exceeding contrast ratios of about 10 percent. The first two methods should be able to reduce minimum contrast by a factor of three or more.

10.3.3 Electronic Noise

Electronic noise in the preamplifiers used with contemporary vidicons poses a problem almost as serious as retina imperfections. All-altitude capability daylight startrackers will not be capable of detection of stars much dimmer than second magnitude against a sky brighter than 1,000 foot-lamberts without drastic reduction in frame rate below five per second, employment of preamplifiers with rms noise currents well below 0.9 by 10^{-12} ampere per cps, or both.

10.3.4 Sky Background Photon Noise

For wide field-of-view startrackers using vidicons, the fundamental limitation due to photon noise from the bright sky background is not a problem in detection of second magnitude stars against 1,000 foot-lambert skies. It will be a problem only when startrackers get down to attempting detection of fourth to fifth magnitude stars against 1,000 foot-lamberts, or third to fourth magnitude against 2,500 foot-lamberts.

10.4 PROCESSING OF IMAGE TUBE OUTPUT

In Section 9 we considered "shuttered" operation of an image tube as a means for overcoming star/sky contrast by image perturbations. This is but one means of overcoming a critical system limitation to ensure mission success. No consideration has been given previously to spatial analysis and/or statistical processing of the photosensor output signal. However, it would be remiss not to mention the possibility of doing such things as frame-to-frame correlation to reduce significantly the minimum detectable contrast ratio. The performance of startracker systems can be influenced strongly by such signal treatment.

Assuming that unlimited time is available for the mission, in principle, both the detectability and the positional location accuracy are independent of the star image size. The ultimate improvement possible by using statistical processing techniques to detect a star signal among the noise sources can be analyzed by information theory, and is proportional to the integration time available. This, in turn, is limited by the sample length over which the noise can be considered to remain a random process.

The primary problem in reducing "detector-scan" noise (i.e., in reducing the minimum detectable contrast ratio due to image tube imperfections) lies in mechanizing the startracker system to enable it to discriminate between a star image and false image detail. In other words, the system must be able to pick out the star signal from the detector-scan noise. Since false image detail always appears in the same pattern on the photocathode, it is obvious that a star whose image remains stationary on the photocathode could be indistinguishable from the noise. Therefore, to distinguish between star and false image detail, the star image in most cases on the photocathode must be in motion (the single exception to this will be discussed in Paragraph 10.4.3). Then the star image will either make a "track" on the exposure, or it will appear in different places in different exposures. In this connection, it may be fortuitous that such image perturbations as platform transients and atmospheric shimmer are present.

Three methods have been identified for accomplishing this and are discussed in Paragraphs 10.4.1, 10.4.2, and 10.4.3. The list is certainly not exhaustive. One or more of these methods should be capable of reducing the minimum detectable contrast ratio resulting from detector scan noise by an order of magnitude.

10.4.1 Signal Subtraction Method*

In this method the star motion on the photocathode is produced by the image perturbation phenomena. Star motion during exposure is effectively stopped during exposure. The signal outputs for two successive frames are recorded. Then the recorded signals from each frame are played back simultaneously into a subtracting circuit which all but eliminates the false image detail, leaving only the two star signals. Such signals, from a number of frame pairs, may then be averaged to reduce star position uncertainty.

10.4.2 Tube-Jitter Method*

This second method introduces motion or displacement of the image tube. Such a technique is used with an essentially time-stationary scene and requires exposures of one second or so. This allows image perturbations to produce well-smeared, stationary, star images having half-widths of about 12 to 15 arc-seconds. Each exposure in a correlated sequence would be made so that the image fell on a slightly different point on the photocathode. This can be accomplished by mechanically or optically displacing the optical axis in a known manner. Finally, the various exposures could be correlated superposing them in a storage tube in such a manner that a given point in the object space is never superposed with any other point. The result is that the star, being time-stationary in the object space, produces an image on each exposure which is superposed. The photocathode imperfections, however, produce false image details which move to different places in the object space for each exposure. These will not superpose, but add incoherently in much the same fashion as random noise.

10.4.3 Point Subtraction Method

Whenever the photocathode irregularities are, by nature, discrete points rather than a continuous function of position throughout the image, a more straightforward method of signal discrimination is possible. If these points are few enough, their coordinates may be stored in a computer memory and used to reject the signals produced by the irregularities.

*These first two methods may be used whenever the detector-scan noise is produced by image irregularities which vary continually over the whole image.

10.5 THE POTENTIALITY OF IMAGE TUBES IN DAYLIGHT STARTRACKERS

The size and complexity of statistical data processing equipment varies widely depending on the amount and type of analysis to be performed. However, it appears possible to effect considerable improvements in startracker performance with equipment not significantly larger in size than the startracker itself. Further effort along this line is recommended to define further the applicable data processing techniques and reduce them to workable concepts. These may be then subjected to more detailed error analyses than is possible at this time.

In any event, the present feasibility of detection of second magnitude stars against 1,000 foot-lambert backgrounds, the future improvement in image tubes, and the performance improvement possible through signal processing, give the image tube a present capability for wide field-of-view daylight startracking and a growth potential unmatched and unattainable by any other photosensor.

REFERENCES

1. McCanless, F., Quasius, G., Unruh, W., "Star Tracker Aerospace Reference Study - STARS"; Technical Documentary Report ASD-TDR-62-1056, St. Petersburg, Florida, Minneapolis-Honeywell Regulator Company, 20 January 1963.

2. Nagel, Max R. (edited by), GRD Research Notes No. 46, "Background Measurements During the Infrared Measuring Program 1956 (IRMP 56)"; Bedford, Massachusetts, Geophysics Research Directorate, AF Cambridge Research Laboratories, November 1960.

3. Nettelblad, F., "Studies of Astronomical Scintillation"; Sweden, Lund Observatory Publication, Series II, No. 130, 1953.

4. Brown, Duane C., RCA Data Reduction Technical Report No. 39, "A Treatment of Analytical Photogrammetry with Emphasis on Ballistic Camera Applications"; Arlington, Virginia, Armed Services Technical Information Agency, AD 124144, 20 August 1957.

5. Hosfeld, Roger, "Comparisons of Stellar Scintillation with Image Motion"; Journal of the Optical Society of America, Volume 44, Number 4, Delaware, Ohio, Perkins Observatory, April 1954.

6. Hynek, J. Allen, "On the Effects of Image Motion on the Accuracy of Measurement of a Flashing Satellite"; Special Report No. 33, Cambridge, Massachusetts, Smithsonian Institution Astrophysical Observatory, 1 February 1960.

7. Lorah, Lawrence D., "Some Influences of Near-Field Aerodynamics on Optical Equipment"; Wind Tunnel Report 422, Cambridge, Massachusetts, Massachusetts Institute of Technology, Naval Supersonic Laboratory, June 1960.

8. USN - USL Report No. 522 1-200-00-00, Fort Trumbull, New London, Connecticut, US Navy Underwater Sound Lab, 10 August 1961.

9. Milligan, G. M., Letter to B. F. Conroy, Fort Trumbull, New London, Connecticut, US Navy Underwater Sound Laboratory, 1 February 1963.

10. Free, L. J., "Wiener Spectra Measurements by USNUSL During IRMP 59/60 at Patrick Air Force Base, Florida"; Enclosed as appendix to preceding reference.

11. Cope, A. D., Borkan, H., "Performance and Operation of the Image Isocon Camera Tube"; Arlington, Virginia, Armed Services Technical Information Agency, April 1960, AD249751. Also WADD Technical Note 60-123.

12. Schneeberger, R. J., Skorinko, G., Doughty, D. D., and Fiebelman, W. A., " Electron Bombardment Induced Conducitivity Including its Application to Ultraviolet Imaging in the Schuman Region"; Proceedings of the Image Intensifier Symposium, Fort Belvoir, Virginia, sponsored by NASA, 24-26 October 1961.

13. Not used.

14. Brochure, " Radiation Tracking Transducer XY20"; San Gabriel, California, Micro Systems, Incorporated.

15. Jones, R. Clark, "Quantum Efficiency of Detectors for Visible and Infrared Radiation"; Cambridge, Massachusetts, Research Laboratory, Polaroid Corporation, 1959. Contained in "Advances in Electronics and Electron Physics", Volume XI, 1959. Academic Press, New York and London.

16. Hynek, J. A., Barton G., Aikens, R., and Powers, W., "Potentialities and Limitations of Image Scanning Techniques in Astronomy"; Evanston, Illinois, Dearborn Observatory, Northwestern University, and Organ, New Mexico, Organ Pass Observatory, Northwestern University. Contained in "Advances in Electronics and Electron Physics", Volum XVI, Photo-Electronic Image Devices, 1962, Academic Press, New York and London.

17. DeWitt, Jr., J. H., "A Report on the Image Orthicon Using Slow Read-out", Nashville, Tennessee, Arthur J. Dyer Observatory, Vanderbilt University. Contained in "Advances in Electronics and Electron Physics", Volume XVI, Photo-Electronic Image Devices 1962, Academic Press, New York and London.

18. Livingstone, W. C., "Stellar Photometry with an Image Orthicon"; Tucson, Arizona, Kitt Peak National Observatory. Contained in "Advances in Electronics and Electron Physics", Volume XVI, Photo-Electronic Image Devices, 1962, Academic Press, New York and London.

19. Robe, John K., "Barrier Grid Storage Tube Disturbance"; Report R-103, Urbana, Illinois, Control Systems Laboratory, University of Illinois, August 1958.

20. Robe, John K., "Storage Tube Resolution"; Report R-93, Urbana, Illinois, University of Iilinois, Control Systems Laboratory, March 1957.

21. Not used.

22. "Slow Scan Specification T3, Electron Tube, One-half inch Vidicon, Tube Type C73496B for TIROS and Project 417-A Cameras"; Attachment to a letter to B. Conroy from F. David Marschka, Radio Corporation of America, 11 November 1963.

23. Rose, A., "Television Pickup Tubes and the Problem of Vision"; Princeton, New Jersey, RCA Laboratories Division, 1948. Contained in Advances in Electronics, Volume I, 1948, Academic Press, New York, New York.

24. Brochure, "ML-7351 Vidicon, Description and Ratings"; Machlett Laboratories, Inc., Springdale, Connecticut, February 1961.

25. Gray, Dwight E., (Coordinating Editor), " American Institute of Physics Handbook"; New York, New York, McGraw-Hill Book Company, Inc., 1963.

26. Schade, O. H., "A New System of Measuring and Specifying Image Definition"; Proceedings of the NBS Semicentennial Symposium on Optical Image Evaluation Held at the NBS on 18, 19, 20 October 1951, National Bureau of Standards Circular 526, 29 April 1954.

INDEX INFORMATION SHEET

AL TDR 64-90. ANALYSIS OF THE APPLICATION OF IMAGE-FORMING PHOTOSENSORS TO WIDE FIELD-OF-VIEW DAYLIGHT STAR TRACKERS. 20 August 1964. Unclassified. Honeywell, Aeronautical Division, St. Petersburg, Fla. C AF 33(657)-11694. P 4200. T 420016. SRN Aero Report 664-2 (Honeywell Aero Report 11694-IR3). In DDC. Aval from OTS.

This report analyzes the performance limitations of wide field-of-view (approximately one degree by one degree) daylight star tracking systems employing image-forming photosensors. The star tracker was assumed to be an alignment reference for an inertial guidance system. Assumed system parameters are general enough to make results applicable to both air- and missile-borne applications and to unrestricted operating altitudes.

RCS AFSC-R47